






Mitotic WNT signalling orchestrates neurogenesis in the developing neocortex

Fabio Da Silva^{1,†} , Kaiqing Zhang^{1,†} , Anneline Pinson², Edoardo Fatti^{1,†,‡} , Michaela Wilsch-Bräuninger², Jessica Herbst¹, Valerie Vidal³, Andreas Schedl³, Wieland B Huttner^{2,*}  & Christof Niehrs^{1,4,**} 

Abstract

The role of WNT/ β -catenin signalling in mouse neocortex development remains ambiguous. Most studies demonstrate that WNT/ β -catenin regulates progenitor self-renewal but others suggest it can also promote differentiation. Here we explore the role of WNT/STOP signalling, which stabilizes proteins during G2/M by inhibiting glycogen synthase kinase (GSK3)-mediated protein degradation. We show that mice mutant for cyclin Y and cyclin Y-like 1 (*Ccny/Il1*), key regulators of WNT/STOP signalling, display reduced neurogenesis in the developing neocortex. Specifically, basal progenitors, which exhibit delayed cell cycle progression, were drastically decreased. *Ccny/Il1*-deficient apical progenitors show reduced asymmetric division due to an increase in apical-basal astral microtubules. We identify the neurogenic transcription factors Sox4 and Sox11 as direct GSK3 targets that are stabilized by WNT/STOP signalling in basal progenitors during mitosis and that promote neuron generation. Our work reveals that WNT/STOP signalling drives cortical neurogenesis and identifies mitosis as a critical phase for neural progenitor fate.

Keywords WNT signalling; mitosis; neurogenesis; LRP6; microcephaly

Subject Categories Development; Neuroscience; Signal Transduction

DOI 10.15252/embj.2021108041 | Received 17 February 2021 | Revised 5 August 2021 | Accepted 10 August 2021 | Published online 25 August 2021

The EMBO Journal (2021) 40: e108041

Introduction

During embryonic/foetal development, the mammalian neocortex undergoes a large increase in surface area and a drastic expansion of the number of projection neurons necessary for higher cognitive functions (Caviness *et al.*, 1995; Rakic, 1995; Rakic, 2009; Lui *et al.*, 2011; Florio & Huttner, 2014; Sun & Hevner, 2014). Crucial to this

increase are the neural progenitor cells (NPCs) in the developing neocortex. The primary population of NPCs reside in the ventricular zone (VZ), adjacent to the ventricular lumen, and during the initial stages of neocortex development undergo several rounds of self-amplifying symmetric divisions (Malatesta *et al.*, 2000; Noctor *et al.*, 2001; Götz & Huttner, 2005), commonly referred to as increased self-renewal (see note on terminology in Methods). With the onset of cortical neurogenesis, these NPCs, known as “apical progenitors” (APs), begin to divide asymmetrically to generate either post-mitotic neurons (direct neurogenesis, a minor pathway in mammals) or a secondary population of NPCs termed “basal progenitors” (BPs, indirect neurogenesis, the major pathway in mammals) (Kriegstein & Götz, 2003; Götz & Huttner, 2005; Taverna *et al.*, 2014). In contrast to APs that undergo mitosis at the apical surface, BPs undergo mitosis basal to the VZ in a second germinal zone known as the subventricular zone (SVZ). Depending on the mammalian species, BPs either divide to give rise to two neurons (also referred to as neuronal differentiation of BPs), which is typically the case in embryonic mouse neocortex, or first self-renew to increase their pool size and then generate neurons, which is the case for foetal human neocortex (Lui *et al.*, 2011; Florio & Huttner, 2014; Taverna *et al.*, 2014; Molnár *et al.*, 2019). Maintaining the balance between symmetric self-renewing AP divisions and asymmetric BP-genic AP divisions is one critical basis for generating the correct number of neurons in the neocortex (Huttner & Kosodo, 2005; Delaunay *et al.*, 2017). In this context, cell signalling pathways are crucial to regulate neurogenesis, but pinpointing their precise functions (e.g. in NPC self-renewal vs. generation of differentiated cells, in which cell types, at which developmental stages) has proven challenging, and, at times, controversial (Taverna *et al.*, 2014).

A case in point is WNT signalling, a conserved pathway that is intricately linked with neocortex development. The overall role of WNT signalling in neurogenesis is complex and highly dependent upon the models used, as well as the epistatic level at which the pathway is manipulated (Harrison-Uy & Pleasure, 2012). For

1 Division of Molecular Embryology, DKFZ, Heidelberg, Germany

2 Max Planck Institute of Molecular Cell Biology and Genetics, Dresden, Germany

3 INSERM, CNRS, iBV, Université Côte d'Azur, Nice, France

4 Institute of Molecular Biology (IMB), Mainz, Germany

*Corresponding author. Tel: +49 351 210 1500; E-mail: huttner@mpi-cbg.de

**Corresponding author (lead contact). Tel: +49 6131 3921401; E-mail: niehrs@dkfz-heidelberg.de

†These authors contributed equally to this work as Co-first authors

‡Present address: Department of Biology, Institute of Biochemistry, ETH (Eidgenössische Technische Hochschule), Zürich, Switzerland

instance, genetic ablation of β -catenin, the signal transducer driving the transcriptional response of canonical WNT signalling, leads to increased cell cycle exit of NPCs and premature neuronal differentiation (Machon *et al*, 2003; Woodhead *et al*, 2006; Mutch *et al*, 2010). Conversely, overexpression of constitutively active β -catenin or deletion of glycogen synthase kinase 3 (GSK3), a key negative regulator of canonical WNT signalling, drive increased AP self-renewal at the expense of BP and post-mitotic neuron generation (Chenn & Walsh, 2002; Machon *et al*, 2007; Wrobel *et al*, 2007; Kim *et al*, 2009). Hence, it is generally thought that the primary role of canonical WNT signalling is to promote NPC self-renewal, a phenomenon that is also observed in other parts of the developing nervous system and is mediated by the transcriptional activity of β -catenin (Zechner *et al*, 2003; Gulacsi & Anderson, 2008; Draganova *et al*, 2015). However, *in vitro* studies have demonstrated that WNT/ β -catenin, through transcriptional regulation of N-myc and the neurogenic transcription factors Ngn1/2, can also promote differentiation of NPCs (Hirabayashi *et al*, 2004; Israsena *et al*, 2004; Kuwahara *et al*, 2010). *Wnt7a* and *Wnt7b* promote NPC proliferation (Viti *et al*, 2003; Qu *et al*, 2013). In contrast, mice mutant for LRP6 (low-density lipoprotein receptor-related protein 6), the principle co-receptor for the canonical pathway, exhibit normal NPC proliferation but decreased neuronal differentiation (Zhou *et al*, 2006). Further complicating issues, expression of *Wnt3a* in the neocortex of mouse embryos by *in utero* electroporation leads to both AP self-renewal and neuronal differentiation of BPs (Munji *et al*, 2011).

Taken together, the precise role of WNT signalling in mouse neocortex development remains unclear. Does canonical WNT signalling promote self-renewal or differentiation of NPCs? One solution to the observed discrepancies could be that WNT signalling regulates both progenitor self-renewal and differentiation but in different populations of NPCs, namely self-renewal in APs and differentiation in BPs (Munji *et al*, 2011). However, another possible explanation for the apparent inconsistencies may be that manipulation of WNT signalling components can exert different effects depending on whether the manipulated WNT effectors function upstream or downstream in the pathway. This is because WNT/LRP6 signalling triggers various sub-pathways that are differentially affected by manipulation at the ligand, receptor, or intracellular levels (Acebron & Niehrs, 2016; García de Herreros & Duñach, 2019).

The main function of LRP6-dependent WNT signalling is to inhibit GSK3, and it is still widely assumed that the only relevant GSK3 substrate in the WNT pathway is β -catenin (Nusse & Clevers, 2017). However, in addition to β -catenin, GSK3 can phosphorylate many other proteins and target them for proteasomal degradation (Taelman *et al*, 2010; Acebron *et al*, 2014). In this context, a novel player is the WNT/STOP (WNT-stabilization of proteins) pathway (see Fig EV1A for a model), which acts post-transcriptionally, is independent of β -catenin, peaks during mitosis, and slows down degradation of numerous proteins as cells prepare to divide (Acebron *et al*, 2014). Key effectors of WNT/STOP signalling are cyclin Y (*Ccny*) and cyclin Y-like 1 (*Ccnyl1*), conserved cyclins that together with their cyclin-dependent kinases (CDK) 14 and 16 phosphorylate and activate the WNT co-receptor LRP6 in G2/M. This co-receptor activation leads to a peak of WNT signalling and GSK3 inhibition in mitosis (Davidson *et al*, 2009). *In vivo*, the WNT/STOP

pathway plays a role in germ cells (Huang *et al*, 2015; Koch *et al*, 2015) and cancer cells (Madan *et al*, 2018; Hinze *et al*, 2019).

Here, we examine the *in vivo* role of WNT/STOP signalling in NPCs during multiple phases of mouse neocortex development. Genetic ablation of *Ccny* and *Ccnyl1* leads to a thinner cerebral cortex and a reduced number of BPs and post-mitotic neurons. Importantly, *Ccny/l1*-deficient mice display decreased WNT signalling at the receptor level, but not at the transcriptional level. Through a series of *in vivo* and *in vitro* analyses, we show that WNT/STOP signalling is essential for asymmetric AP division, cell cycle progression of BPs and neuron generation. Mechanistically, *Ccny/l1* stimulate neuronal differentiation of BPs through post-transcriptional regulation of Sox4 and Sox11, two essential neurogenic transcription factors (Bergsland *et al*, 2006; Chen *et al*, 2015) that we identify as direct GSK3 targets. We therefore propose that WNT/STOP signalling is the primary driver of neuronal differentiation of NPCs whereas WNT/ β -catenin signalling predominantly regulates NPC self-renewal.

Results

WNT/STOP signalling is required for neurogenesis in the embryonic mouse neocortex

To study the role of WNT/STOP signalling in the developing mouse neocortex, we generated embryos deficient for *Ccny* and *Ccnyl1* (hereafter referred to as double knockout (DKO) embryos). In contrast to individual *Ccny* or *Ccnyl1*-deficient embryos, which are both viable (An *et al*, 2015; Koch *et al*, 2015), DKO embryos displayed *in utero* death beginning at embryonic day 14.5 (E14.5). To avoid that the results of our analyses of DKO embryos might reflect non-specific effects resulting from early lethality, we analysed DKO and littermate control embryos at E13.5. Analysis of haematoxylin–eosin (HE)-stained DKO forebrains revealed a significantly thinner neocortical wall (−32%, $P = 0.0004$) compared to littermate controls. Mediolateral neocortex length was not significantly changed (Fig 1A; quantified in Appendix Fig S1A and B).

To further dissect the reduction in the thickness of the neocortical wall observed in E13.5 DKO embryos, we measured VZ, SVZ and intermediate zone (IZ) plus cortical plate (CP) thickness upon DNA staining and immunofluorescence microscopy (IF) for T-box brain protein 2 (*Tbr2*), a BP marker that permitted visualization of the SVZ. This revealed that within the thinner neocortical wall of DKO embryos, the proportion of neocortical wall thickness constituted by the VZ was increased by 12%, whereas that constituted by the SVZ and IZ+CP was decreased by 20% and 18%, respectively, when compared to the respective proportions in the thicker neocortical wall of control embryos (Fig 1B and C; Appendix Fig S1C and F).

To corroborate these observations, we quantified the number of APs, BPs and post-mitotic deep-layer neurons upon IF for their respective markers Paired box protein 6 (*Pax6*), *Tbr2*, and T-box brain protein 1 (*Tbr1*). The percentage of *Pax6*⁺ cells in the thinner neocortex of E13.5 DKO embryos was slightly increased (+11%, $P = 0.04$) whereas the percentages of *Tbr2*⁺ and *Tbr1*⁺ cells were decreased (−38%, $P = 0.0006$; −25%, $P = 0.01$; respectively) when compared to the thicker neocortex of control embryos (Fig 1D–I).

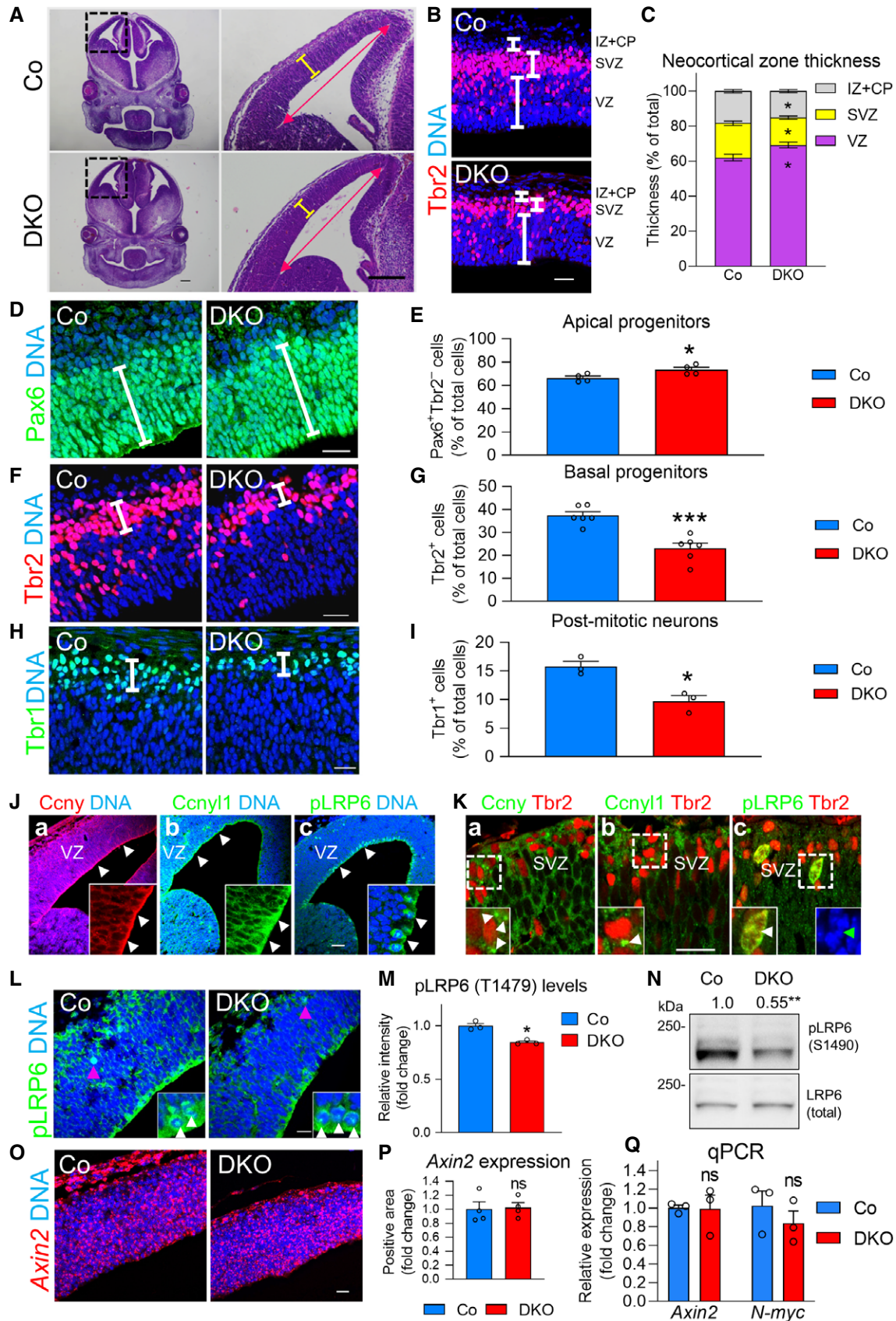


Figure 1.

Figure 1. WNT/STOP signalling is required for neurogenesis in the embryonic mouse neocortex.

- A Haematoxylin and eosin (HE) staining on sections of the neocortex from control (Co) and cyclin Y (*Ccny*) and cyclin Y-like 1 (*Ccnyl1*) double knockout (DKO) embryos at E13.5. Neocortex thickness (indicated by yellow bars) is reduced in DKO vs. control embryos while mediolateral neocortex length (indicated by pink arrows) does not display obvious differences. Scale bars 100 μ m.
- B Hoechst (DNA) staining and IF for Tbr2 to calculate the thickness (white bars) of the VZ, SVZ and intermediate zone + cortical plate (IZ+CP) in control and DKO E13.5 neocortex. Scale bar 20 μ m.
- C Quantification of VZ, SVZ and IZ+CP thickness in control and DKO E13.5 neocortex. Each zone is represented as percentage of total thickness (measured in μ m) of the neocortex. Columns are means \pm SEM ($n = 6$ embryos, 4 litters).
- D IF for Pax6 and Tbr2 (not shown) in control and DKO E13.5 neocortex. White bars indicate thickness of Pax6⁺ zone (i.e. VZ). Scale bar 20 μ m.
- E Quantification of the number of APs (Pax6⁺Tbr2⁻) from (D). Pax6⁺Tbr2⁺ cells were excluded from final counts. AP numbers are expressed as percentage of total cell number (sum of D, F and H). Columns are means \pm SEM ($n = 4$ embryos, 3 litters).
- F IF for Tbr2 in control and DKO E13.5 neocortex. White bars indicate thickness of Tbr2⁺ zone (i.e. SVZ). Scale bar 20 μ m.
- G Quantification of the number of BPs from (F). Columns are means \pm SEM ($n = 6$ embryos, 3 litters).
- H IF for Tbr1 in control and DKO E13.5 neocortex. White bars indicate thickness of Tbr1⁺ zone (i.e. mostly CP). Scale bar 15 μ m.
- I Quantification the number of deep-layer post-mitotic neurons from (H). Columns are means \pm SEM ($n = 3$ embryos, 3 litters).
- J IF for *Ccny* (a), *Ccnyl1* (b) and LRP6 (c) (low-density lipoprotein receptor-related protein 6) phosphorylated at T1479 (pLRP6) in the neocortex of E13.5 control embryos. White arrowheads in (a,b) indicate apical membrane / cortex, shown at higher magnification in the insets. High levels of LRP6 phosphorylation are detected in mitotic APs (c, white arrowheads). Scale bar 50 μ m.
- K IF for *Ccny*(a), *Ccnyl1*(b) and pLRP6(c), each together with IF for Tbr2, in the neocortex of E12.5 control embryos. White arrowheads in the insets of (a, b) depict *Ccny*/*l1* puncta in Tbr2⁺ BPs. High levels of LRP6 phosphorylation are detected in mitotic BPs (c, inset, white arrowhead). DNA staining for mitotic pLRP6⁺ BP shown in bottom right inset (c, green arrowhead). Scale bar 20 μ m.
- L IF for pLRP6 (T1479) in the neocortex of E13.5 control and DKO embryos. White arrowheads depict mitotic APs and purple arrowheads depict mitotic BPs. Scale bar 20 μ m.
- M Quantification of relative pLRP6 staining intensity in mitotic APs and BPs from (L). Data are expressed as fold change vs. controls and are means \pm SEM ($n = 3$ embryos, 3 litters).
- N Immunoblot analysis with an antibody against LRP6 phosphorylated at S1490 (pLRP6 (S1490)) of protein lysates from E13.5 control and DKO forebrains. Numbers above blot indicate fold change vs. controls of phospho-LRP6 (S1490) protein levels normalized to total LRP6 ($n = 6$ embryos, 3 litters).
- O Expression analysis of the β -catenin target gene *Axin2* by *RNAScope in situ* hybridization on neocortex sections from E13.5 control and DKO embryos. Scale bar 20 μ m.
- P Quantification of (O). *Axin2*⁺ area was calculated and normalized to total neocortex area. Data are expressed as fold change vs. controls and are means \pm SEM ($n = 4$ embryos, 3 litters).
- Q *Axin2* and *N-myc* qPCR expression analysis on RNA extracted from E13.5 dorsal forebrains. Data are expressed as fold change vs. controls and are means \pm SEM ($n = 3$ embryos, 2 litters).

Data information: Unpaired two-tailed t-test for all statistical analyses: ns, not significant; * $P < 0.05$, ** $P < 0.01$, *** $P < 0.001$. $P = 0.00040$ (A); $P = 0.016$ (C, VZ); $P = 0.031$ (C, SVZ); $P = 0.042$ (C, IZ +CP); $P = 0.039$ (E); $P = 0.00060$ (G); $P = 0.011$ (I); $P = 0.010$ (M); $P = 0.0010$ (N); $P = 0.85$ (P); $P = 0.95$ (Q, *Axin2*); $P = 0.41$ (Q, *N-myc*)
Source data are available online for this figure.

Consistent with this, IF for β III-tubulin (Tuj1), which marks newborn neurons, revealed that in the thinner neocortical wall of E13.5 DKO embryos, the layers containing newborn neurons comprised a lesser proportion of the neocortical wall thickness than in the thicker neocortical wall of control embryos (control 50.9 ± 5.5 vs. DKO 33.2 ± 1.0 (% of total cortex thickness), $P = 0.048$; Fig EV1B). Together, these data indicated that the reduction in neocortical wall thickness in E13.5 DKO embryos was primarily due to a decrease in the levels of BPs and newborn neurons, which in turn suggested that cortical neurogenesis is reduced in DKO embryos.

Decreased BP and, consequently, post-mitotic neuron levels can be due, at least in part, to structural defects in neocortical cytoarchitecture, such as improper organization of the radial glial scaffold and disruption of apical-basal polarity, which may impede migration of BPs to the SVZ and of newborn neurons to the CP (Taverna *et al*, 2014). However, IF against the radial glia-specific intermediate filament marker nestin revealed no overt abnormalities in the radial glial scaffold of E13.5 DKO neocortex when compared to control (Fig EV1C). Also, we observed normal enrichment of β -catenin at the apical cell cortex of DKO forebrains, suggesting that apical-basal polarity was not affected in the absence of *Ccny*/*l1* (Fig EV1D). We conclude that DKO embryos display neurogenesis defects but no major structural abnormalities in the embryonic neocortex.

We performed IF for *Ccny* and *Ccnyl1* in the E12.5-13.5 mouse neocortex. Interestingly, both *Ccny* and *Ccnyl1* immunoreactivity was concentrated at the apical cell cortex/apical plasma membrane of the VZ of control embryos (Fig 1J-a,b). No *Ccny* or *Ccnyl1* immunoreactivity was detected in the neocortex of DKO embryos, confirming that the two polyclonal *Ccny* and *Ccnyl1* antibodies used are specific (Fig EV1E and F). *Ccny* and *Ccnyl1* immunoreactivity was also detected in, respectively, $28 \pm 0.63\%$ and $24 \pm 0.68\%$ of Tbr2⁺ BPs in the SVZ (Fig 1K-a,b). *Ccny*/*l1* were not detected in post-mitotic neurons. To further analyse the distribution of *Ccny*/*l1* protein in APs and BPs, we performed *in utero* electroporation (IUE) in E13.5 embryos with a plasmid coding for green fluorescent protein (GFP) and analysed embryos at E15.5. Triple IF for *Ccny*/*l1*, the AP marker Sox2 (SRY (sex determining region Y)-2), and GFP confirmed *Ccny*/*l1* immunoreactivity at the apical membrane of electroporated APs (Fig EV1G), while triple IF for *Ccny*/*l1*, Tbr2 and GFP revealed *Ccny*/*l1* immunoreactivity as single puncta in BPs (Fig EV1H). In light of these observations, we next performed IF with an LRP6 antibody specific for the casein kinase 1 gamma (CK1 γ) phosphorylation site T1479, which marks active WNT signalling (Davidson *et al*, 2005). Similar to the *Ccny* and *Ccnyl1* immunoreactivity, phospho-T1479 LRP6 immunoreactivity was also found to be concentrated at the apical cell cortex / apical plasma membrane of the VZ of E13.5 control mouse neocortex (Fig 1J-c). This concentration reflected the specific enrichment of phospho-

LRP6 immunoreactivity in 91% of mitotic APs analysed (Fig 1J-c, arrowheads, inset). The apical concentration of phospho-LRP6 immunoreactivity in mitotic APs is consistent with the fact that mitosis of APs typically occurs at the ventricular surface of the neocortex (Taverna *et al*, 2014). Phospho-T1479 LRP6 immunoreactivity was also observed in 48% of mitotic BPs of E12.5 control mouse neocortex (Fig 1K-c, inset). To confirm this pattern of immunostaining, we performed IF on control embryonic mouse neocortex with another phospho-LRP6 antibody that detects the CDK14 priming phosphorylation site S1490 (Davidson *et al*, 2009). Again, phospho-S1490 LRP6 immunoreactivity was enriched in E13.5 mitotic APs (90%) and BPs (88%), with the mitotic stage of these progenitors being confirmed by co-immunostaining with the mitotic marker phospho-histone H3 (pHH3) (Fig EV1I, insets and arrowhead). Mitotic APs also showed Ccny (30%) and Ccny11 (29%) immunoreactivity (Fig EV1J). IF for total LRP6, CDK14 and GSK3 β revealed the greatest concentration of immunoreactivity at the apical cell cortex / apical plasma membrane of the VZ of E13.5 control mouse neocortex (Fig EV1K). Altogether, these data suggest that the core components of the WNT/STOP signalling pathway are expressed in the embryonic mouse neocortex and that WNT/LRP6 signalling peaks during mitosis in APs and BPs.

To determine whether WNT signalling in DKO forebrains was affected at the receptor level, we quantified the immunostaining intensity for active phospho-LRP6 (T1479) within mitotic APs and BPs of the E13.5 neocortex and detected a decrease (-15% , $P = 0.01$) when compared to controls (Fig 1L and M). Phosphorylation of LRP6 at S1490 was even more markedly reduced (-45% , $P = 0.001$) when analysed by immunoblotting of protein lysates extracted from E13.5 DKO and control forebrains (Fig 1N). To monitor canonical WNT signalling, we performed *RNAscope* analysis on sections of E13.5 neocortex using a probe against the β -catenin target gene *Axin2*. *Axin2* expression was not significantly changed in the neocortex of DKO embryos when compared to controls (Fig 1O and P). To confirm this result, we extracted RNA from E13.5 dorsal forebrains and performed qPCR analysis. Expression of *Axin2* and *N-myc*, another WNT target gene in the neocortex (Kuwahara *et al*, 2010), was not significantly altered in DKO dorsal forebrains (*Axin2*, $P = 0.95$; *N-myc*, $P = 0.41$) (Fig 1Q). Furthermore, immunoblot analysis of whole forebrain lysates probed with an antibody against dephosphorylated β -catenin, which represents its active form, showed no significant change in E13.5 DKO embryos (Fig EV1L). We conclude that combined *Ccny/11* deficiency in the embryonic mouse neocortex leads to decreased LRP6 receptor activation without changes in β -catenin activity. Together with the reduction in neuron levels in the DKO neocortex, these data are consistent with WNT/STOP signalling being required for neurogenesis in the embryonic mouse neocortex.

DKO embryos show delayed cell cycle progression and increased mitosis length in BPs

In light of the reduced levels of BPs and neurons in the neocortex of DKO embryos, we analysed cell cycle parameters of APs and BPs in control and DKO embryos, as alterations in cell cycle progression have been shown to affect NPC fate and cortical neurogenesis (Götz & Huttner, 2005; Dehay & Kennedy, 2007; Arai *et al*, 2011; Borrell & Calegari, 2014). To label NPCs in S-phase in the neocortex of control

and DKO embryos, we injected the thymidine analog bromo-deoxyuridine (BrdU) at E11.5, E12.5 and E13.5 and sacrificed mice 1 h later. Co-IF for Pax6, Tbr2 and BrdU did not reveal any major difference between control and DKO neocortex in the proportion of APs (Pax6⁺ Tbr2⁻) that were in S-phase (i.e. BrdU⁺) at E11.5 and E12.5, although a slight increase was detected for DKO neocortex at E13.5 (Fig 2A and B). The average percentage of E13.5 BrdU⁺ APs, i.e. APs in S-phase, was 31% for control and 39% for DKO neocortex (Fig 2C). The proportion of BPs (Tbr2⁺) that were in S-phase (BrdU⁺) was moderately decreased in DKO neocortex compared to control at all time points analysed (Fig 2D and E). The average percentage of E13.5 BrdU⁺ BPs, i.e. BPs in S-phase, was 24% for control and 21% for DKO neocortex (Fig 2F).

We next determined the length of S-phase of APs and BPs in E13.5 control and DKO neocortex. To this end, we performed timed injections of the thymidine analogs iodo-deoxyuridine (IdU) and BrdU. Briefly, IdU was injected at $T = 0$ to label APs and BPs in S-phase, and BrdU was injected at $T = 1.5$ h to identify those APs and BPs that were still in S-phase at this time vs. those that had left S-phase. Embryos were collected 30 min after BrdU injection (Fig 2G, schematic). We then extrapolated from the percentage of APs (Tbr2⁻) and BPs (Tbr2⁺) of control and DKO neocortex that were IdU⁺ but BrdU⁻, i.e. that had left S-phase after 1.5 h (Fig 2H, yellow; Appendix Fig S1G and H), and determined the time when all control and DKO APs and BPs would have left S-phase, which yielded the length of S-phase for control and DKO APs and BPs (Fig 2I). This revealed a small increase in S-phase length of E13.5 DKO APs as compared to control APs, and a $\approx 50\%$ increase in S-phase length of E13.5 DKO BPs as compared to control BPs (Fig 2I).

Knowing the percentage values of E13.5 control and DKO APs and BPs in S-phase (Fig 2C and F), and the length of S-phase of these types of NPCs (Fig 2I), allowed us to calculate the total length of the cell cycle of E13.5 control and DKO APs and BPs by dividing the S-phase length values (Fig 2I) by the percentage values for these NPCs in S-phase (Fig 2C and F) and then multiplying the resulting numbers with 100 (Fig 2J). This revealed no difference between E13.5 control and DKO APs, but a nearly doubling of total cell cycle length in DKO BPs as compared to control (Fig 2J).

To calculate the length of mitosis, we first performed co-IF for pHH3, Ki67 and Tbr2 (Fig 2K) to determine the percentage of cycling (Ki67⁺) E13.5 control and DKO APs (Tbr2⁻) and BPs (Tbr2⁺) that were in mitosis (pHH3⁺) (Fig 2L). This revealed no major differences between control and DKO APs, nor between control and DKO BPs (Fig 2L). We then calculated the length of mitosis of E13.5 control and DKO APs and BPs by multiplying the total cell cycle length values for each of these NPCs (Fig 2J) with the percentage values for the respective NPC in mitosis (Fig 2L) and divided the resulting numbers by 100, which yielded the length of mitosis (Fig 2M). While no significant difference in mitosis length was found between control and DKO APs, mitosis length of DKO BPs was found to be more than doubled as compared to control (Fig 2M). Data consistent with these findings were obtained when the proportion of APs and BPs in mitosis, deduced from ventricular and abventricular pHH3⁺ cells, respectively, were compared between E11.5-E13.5 control and DKO neocortex (Fig EV2A-C). All cell cycle calculations are detailed in the Appendix Methods.

Mitotic delay can lead to cell cycle arrest and increased apoptosis (Chen *et al*, 2014; Pilaz *et al*, 2016). To compare apoptosis levels in

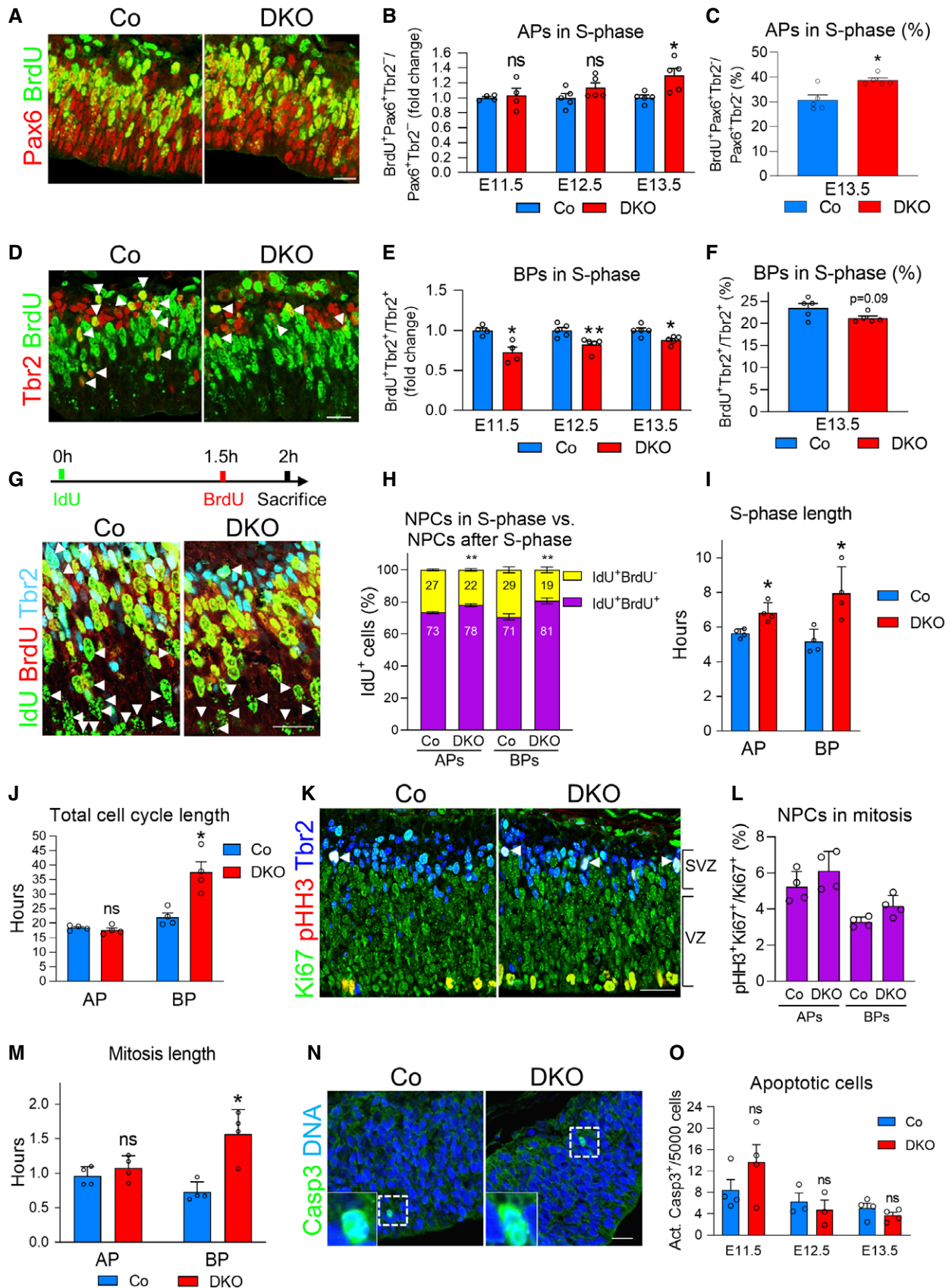


Figure 2.

Figure 2. DKO embryos show delayed cell cycle progression and increased mitosis length in BPs.

- A Triple-IF for BrdU, Pax6 and Tbr2 (not shown) in E12.5 control and DKO neocortices. BrdU was injected into pregnant dams 1 h before sacrifice.
- B Quantification of the proportion of Pax6⁺Tbr2⁻ cells that are BrdU⁺, in control and DKO neocortices at E11.5, E12.5 and E13.5. Data are expressed as fold change vs. controls, with the control values set to 1.0, and are means ± SEM (E11.5 *n* = 4 embryos, 3 litters; E12.5 *n* = 5 embryos, 5 litters and E13.5 *n* = 5 embryos, 4 litters).
- C Average percentage of APs (Pax6⁺Tbr2⁻) (from B) that are BrdU⁺, in E13.5 control and DKO neocortices. Data are means ± SEM.
- D Co-IF for Tbr2 and BrdU (double-positive cells depicted by white arrowheads) in E12.5 control and DKO neocortices. BrdU was injected into pregnant dams 1 h before sacrifice.
- E Quantification of the proportion of Tbr2⁺ cells that are BrdU⁺, in control and DKO neocortices at E11.5, E12.5 and E13.5. Data are expressed as fold change vs controls, with the control values set to 1.0, and are means ± SEM (E11.5 *n* = 4 embryos, 3 litters; E12.5 *n* = 5 embryos, 5 litters and E13.5 *n* = 5 embryos, 4 litters).
- F Average percentage of BPs (Tbr2⁺) (from E) that are BrdU⁺, in E13.5 control and DKO neocortices. Data are means ± SEM.
- G Double IdU/BrdU injection strategy used to calculate S-phase length. Top, scheme. Bottom, triple IF for IdU/BrdU/Tbr2 to detect APs (Tbr2⁻) and BPs (Tbr2⁺) that have exited S-phase (IdU⁺/BrdU⁻, white arrowheads) in control and DKO E13.5 neocortices.
- H Average percentages (numbers in bar graphs) of the IdU⁺ cells that are either BrdU⁺ or BrdU⁻, scored as in (G), for control and DKO APs and BPs. Data are means ± SEM (*n* = 4 embryos, 3 litters).
- I S-phase length of E13.5 control and DKO APs and BPs, calculated from the data of panel (H, yellow) as described in Appendix Methods. Data are means ± SEM (*n* = 4 embryos, 3 litters).
- J Total cell cycle length of E13.5 control and DKO APs and BPs, calculated from the data of panels (C), (F) and (I) as described in Appendix Methods. Data are means ± SEM (*n* = 4 embryos, 3 litters).
- K Co-IF for the proliferation marker Ki67, the mitotic marker phospho-histone H3 (pHH3), and Tbr2 to identify mitotic APs (division at apical surface) and BPs (division in basal VZ or SVZ) in control and DKO E13.5 neocortices. Arrowheads depict pHH3⁺Tbr2⁺ cells.
- L Average percentage of Ki67⁺ APs and BPs that are pHH3⁺ in control and DKO E13.5 neocortices. Data are means ± SEM (*n* = 4 embryos, 3 litters).
- M Mitosis length of E13.5 control and DKO APs and BPs, calculated from the data of panels (J) and (L) as described in Appendix Methods. Data are means ± SEM (*n* = 4 embryos, 3 litters).
- N IF for cleaved caspase 3 (Casp3) to identify apoptotic cells in E13.5 control and DKO neocortices.
- O Quantification of apoptotic cells in control and DKO neocortices at E11.5, E12.5 and E13.5. Data are represented as number of Casp3⁺ cells per 5000 cells. Data are means ± SEM (E11.5 *n* = 4 embryos, 3 litters; E12.5 *n* = 3 embryos, 3 litters, and E13.5 *n* = 4 embryos, 3 litters).

Data information: All scale bars 20 μm. Unpaired two-tailed t-test for all statistical analyses: ns, not significant; **P* < 0.05, ***P* < 0.01. *P* = 0.77 (B, E11.5); *P* = 0.16 (B, E12.5); *P* = 0.030 (B, E13.5); *P* = 0.014 (C); *P* = 0.017 (E, E11.5); *P* = 0.010 (E, E12.5); *P* = 0.013 (E, E13.5); *P* = 0.089 (F); *P* = 0.0069 (H, APs); *P* = 0.0078 (H, BPs); *P* = 0.018 (I, AP); *P* = 0.027 (I, BP); *P* = 0.43 (J, AP); *P* = 0.016 (J, BP); *P* = 0.35 (M, AP); *P* = 0.012 (M, BP); *P* = 0.24 (O, E11.5); *P* = 0.56 (O, E12.5); *P* = 0.26 (O, E13.5). Source data are available online for this figure.

DKO vs. control forebrains, we performed IF with an antibody against cleaved caspase 3 (Fig 2N). Except for a minor, however statistically not significant, increase at E11.5, apoptosis levels in the E12.5 and E13.5 neocortex of DKO embryos were unchanged when compared to controls (Fig 2O). This was confirmed by TUNEL staining, which at E13.5 was also not significantly altered in the neocortex of DKO embryos (Fig EV2D). Thus, apoptosis is unlikely to explain reduced thickness of the cortical plate in DKO embryos. We conclude that the reduction in DKO embryos of cortical plate thickness involves delayed cell cycle progression and increased mitosis length in BPs.

Lack of *Ccny/ll1* expression reduces asymmetric AP division and neurogenesis in the embryonic neocortex

The relative increase in the thickness of the VZ and the reduced BP levels in DKO embryos raised the possibility that their thinner neocortex was not only due to a delayed cell cycle progression of BPs. Instead, the results suggested that *Ccny/ll1* may affect the generation of BPs from APs, and consequently of post-mitotic neurons. In the mammalian neocortex, the switch of APs from symmetric, proliferative divisions to asymmetric, BP-genic divisions is often associated with changes in apical membrane distribution, whereby unequal inheritance of the apical plasma membrane by the daughter cells indicates an asymmetric mode of AP division (Kosodo et al, 2004; Delaunay et al, 2017). We quantified the number of symmetrically vs. asymmetrically dividing APs by IF using the “cadherin hole” method, which allows determination of the plane of division in mitotic APs (Fig 3A) (Kosodo et al, 2004). Interestingly, E13.5 DKO neocortex displayed a 36% reduction in asymmetric AP

division (from 47 to 30% of all AP division, Fig 3B), consistent with decreased generation of BPs in the absence of *Ccny/ll1*.

Mitotic spindle orientation is critical for determining symmetric vs. asymmetric cell division of NPCs in the developing neocortex (Konno et al, 2008; Yingling et al, 2008; Lizarraga et al, 2010; Asami et al, 2011; LaMonica et al, 2013; Xie et al, 2013; Mora-Bermúdez & Huttner, 2015), with a key role of astral microtubules (aMTs) (Mora-Bermúdez et al, 2014). A specific subpopulation of aMTs, which reach the apical or basal cell cortex and are referred to as apical-basal aMTs, are more abundant in symmetrically dividing APs than in asymmetrically dividing APs (Mora-Bermúdez et al, 2014). These apical-basal aMTs promote a mitotic spindle orientation perpendicular to the apical-basal axis of APs and reduce the variability of mitotic spindle orientation, which in turn favours symmetric AP division (Mora-Bermúdez et al, 2014). Perturbations specifically of these apical-basal aMTs increases asymmetric BP-genic APs divisions and neurogenesis (Mora-Bermúdez et al, 2014). To examine aMT abundance, we performed IF for α-tubulin, acquired Z-stack images of dividing APs and quantified the number of apical-basal aMTs vs. the aMTs reaching the central cell cortex (central aMTs) (Fig 3C). Strikingly, E13.5 DKO APs exhibited an increase specifically in apical-basal, but not central, aMTs (Fig 3D), providing a mechanistic explanation for the increase in symmetric AP division (Fig 3B). We conclude that in dividing APs, lack of *Ccny/ll1* expression results in an increase in the number of apical-basal aMTs, which reduces asymmetric, BP-genic cell division and hence neurogenesis in the embryonic neocortex.

DKO embryos display premature embryonic lethality, limiting our analysis of neurogenesis to early stages of development in which the cortical plate is less developed. To analyse the effect of

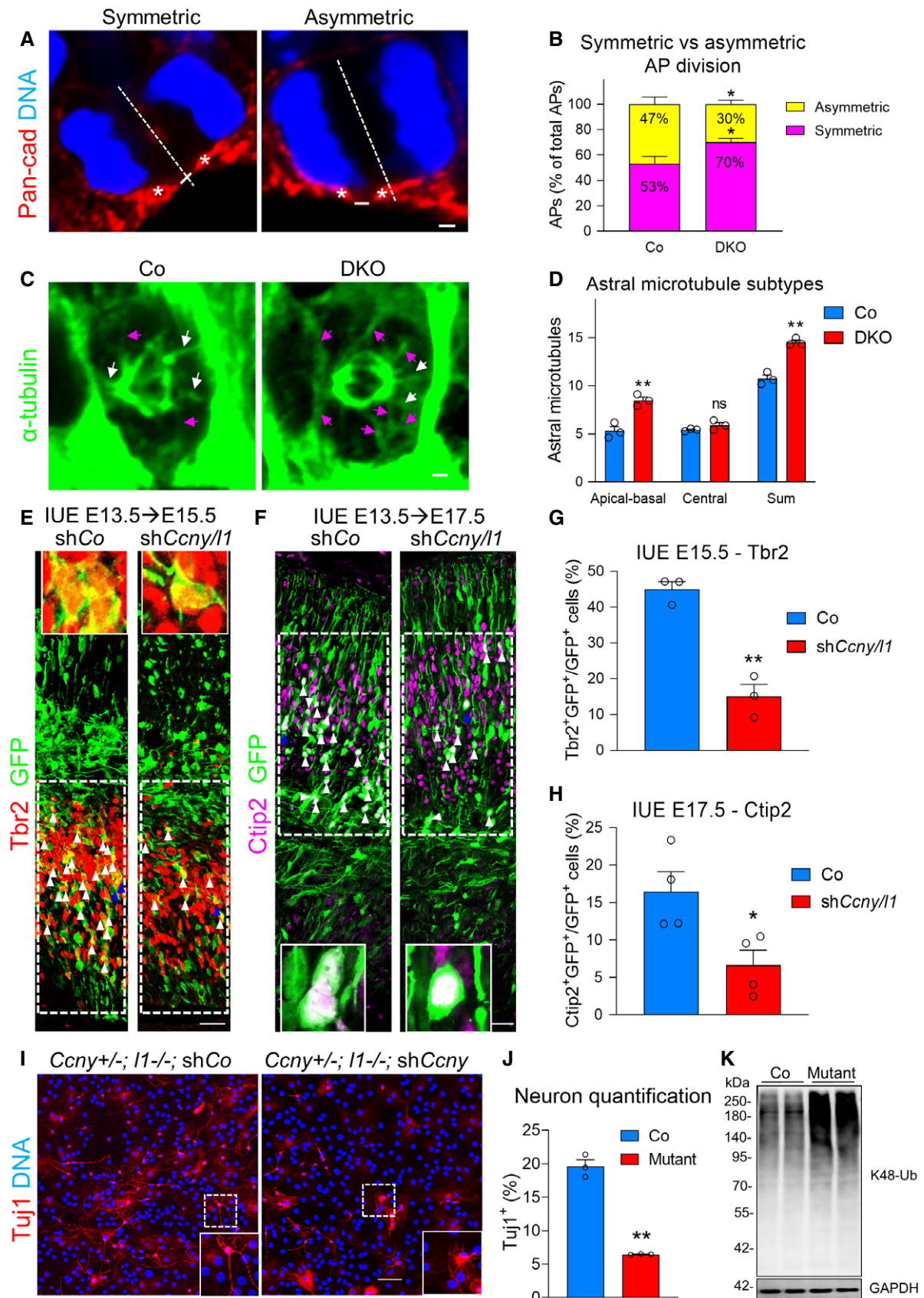


Figure 3.

Figure 3. Lack of *Ccny/11* expression reduces asymmetric AP division and neurogenesis in the embryonic neocortex.

- A IF for pan-cadherin, combined with DNA staining, to quantify asymmetric vs. symmetric division in VZ APs. Dashed white lines denote the cleavage plane, and solid lines mark the “cadherin hole”. Asterisks mark the apical-most basolateral membrane flanking the “cadherin hole”. Cell divisions were scored as symmetric or asymmetric when the cleavage plane bisects (left) or bypasses (right) the cadherin hole, respectively. Scale bar 2 μm .
- B Quantification of symmetric vs. asymmetric AP division in E13.5 control and DKO neocortices, expressed as percentage of total AP divisions. Four independent embryos per genotype from 3 litters were analysed. A total of 110 and 99 cells were counted for controls and DKOs, respectively. Data are means \pm SEM.
- C IF for alpha-tubulin to visualize mitotic spindle and astral microtubules in E13.5 control and DKO neocortices. Central and apical–basal astral microtubules denoted by white and purple arrows, respectively. Scale bar 2 μm .
- D Quantification of apical–basal, central and total (sum) number of astral microtubules in mitotic APs of control and DKO E13.5 neocortices. Data are means of microtubules per cell \pm SEM (at least 10 cells counted per embryo)($n = 3$ embryos, 3 litters).
- E, F *In utero* electroporation (IUE) of plasmids expressing GFP plus shControl (Co) or sh*Ccny/11* into the lateral ventricles of E13.5 wild-type embryos, followed by analysis at E15.5 or E17.5. (E) IF for GFP and Tbr2 in the E15.5 neocortex. (F) IF for GFP and the deep-layer neuron marker CtIP2 in the E17.5 neocortex. (E, F) White arrowheads denote double-positive cells. Insets of magnified cells (indicated by blue arrowheads) depict representative GFP + Tbr2 (E) or GFP + CtIP2 (F) co-staining. Scale bars 20 μm .
- G Quantification of the percentage of GFP⁺ cells that are Tbr2⁺, in control and sh*Ccny/11* neocortices at E15.5 upon IUE at E13.5. Data are means \pm SEM ($n = 3$ embryos).
- H Quantification of the percentage of GFP⁺ cells that are CtIP2⁺, in control and sh*Ccny/11* neocortices at E17.5 upon IUE at E13.5. Data are means \pm SEM ($n = 4$ embryos).
- I IF for β III-tubulin (Tuj1) of control (*Ccny*^{+/-}; *Ccny11*^{-/-}; shRNA Co) and mutant (*Ccny*^{+/-}; *Ccny11*^{-/-}; shRNA *Ccny*) NPC monolayer cultures grown in differentiation medium for seven days. Insets depict neurons with representative neurite morphology for controls and mutants. Scale bar 20 μm .
- J Quantification of the percentage of Tuj1⁺ cells from (I). Data are means \pm SEM (experiment performed twice in triplicates, representative experiment shown).
- K Immunoblot analysis of protein lysates extracted from control and mutant NPCs prior to culture in differentiation medium, using an antibody against lysine 48-ubiquitin (K48-Ub) to label polyubiquitinated proteins targeted for proteasomal degradation. GAPDH, loading control. Two representative samples per genotype are shown.

Data information: Unpaired two-tailed t-test for all statistical analyses: ns, not significant; * $P < 0.05$, ** $P < 0.01$. $P = 0.034$ (both asterisks) (B); $P = 0.0062$ (D, apical-basal); $P = 0.22$ (D, central); $P = 0.0022$ (D, sum); $P = 0.0030$ (G); $P = 0.030$ (H); $P = 0.0053$ (J).

Source data are available online for this figure.

Ccny/11 knockdown in NPCs at later time points, we performed IUE of mouse embryos at E13.5 with plasmids coding for either a control shRNA (Co) or shRNAs against *Ccny* and *Ccny11* (sh*Ccny/11*), along with a plasmid coding for GFP. At E15.5, knockdown of *Ccny/11* greatly reduced the proportion of the GFP⁺ progeny of the electroporated cells that were Tbr2⁺, i.e. BPs (Fig 3E and G). Similarly, at E17.5, the proportion of the GFP⁺ progeny of the electroporated cells that expressed the deep-layer neuron marker CtIP2 was depleted (Fig 3F and H). Altogether, these data corroborate that lack of *Ccny/11* expression reduces neurogenesis in the embryonic mouse neocortex and show that this effect is consistent throughout embryonic development. The IUE results also exclude the possibility that the neurogenesis defect observed in DKO embryos is due to an overall delay in embryonic development, or results from indirect effects related to global deletion of *Ccny/11*.

We next asked whether NPCs deficient for *Ccny/11* also display a reduced capacity to generate neurons *in vitro*. To this end, we isolated NPCs from E13.5 *Ccny*^{+/-}; *Ccny11*^{-/-} forebrains and transduced them with a lentivirus expressing shRNA against *Ccny* (hereafter referred to as mutant NPCs) to induce acute *Ccny/11* deficiency. NPCs were then cultured in differentiation media to promote neurogenesis. IF for Tuj1 revealed a drastic decrease in the percentage of cells expressing this marker of newborn neurons derived from the mutant NPCs, as well as a significant reduction in neurite length (control $47.7 \pm 1.4 \mu\text{m}$ vs. mutant $23.8 \pm 1.8 \mu\text{m}$, $P = 0.0006$; Fig 3I and J). The defect in neuron generation was confirmed by qPCR analysis, which demonstrated a major decrease of the neuronal markers *Tuj1* and doublecortin in mutant NPC cultures (Fig EV3A and B). The neural stem cell marker *Sox2* showed a slight but not significant increase in mutant cells (Fig EV3C). Levels of phospho-LRP6 (S1490), marking active WNT receptor signalling, were drastically reduced, whereas *Axin2* expression was not

significantly altered in the mutant NPC cultures, confirming that the effects of *Ccny/11* during *in vitro* differentiation are independent of canonical WNT/ β -catenin signalling (Fig EV3D and E). Furthermore, immunoblotting of total protein lysates from mutant NPCs showed overall strongly increased lysine-48 ubiquitination (Fig 3K), indicating globally enhanced protein degradation, a hallmark of impaired WNT/STOP signalling (Taelman *et al*, 2010; Acebron *et al*, 2014). The results provide further support that *Ccny/11* and WNT/STOP signalling promote asymmetric AP division and neurogenesis in the embryonic neocortex.

Sox4/11 are direct GSK3 targets

WNT/STOP signalling acts by protecting proteins carrying GSK3 phosphodegrons from proteasomal degradation. To identify downstream targets of WNT/STOP signalling, we screened for effector proteins with a role in neurogenesis and neuronal differentiation that harbour potential GSK3 phosphorylation sites. Two candidates were the SRY-related high-mobility-group box proteins *Sox4* and *Sox11*, SoxC subclass transcription factors. *Sox4/11* display pan neuronal activity and are indispensable for neurogenesis and neuronal differentiation (Bergsland *et al*, 2006). *Sox4* is highly expressed by BPs, and *Sox11* is expressed both by BPs and newly formed neurons (Chen *et al*, 2015). Conditional inactivation of *Sox4* in the neuroepithelium leads to a strong reduction of BPs while *Sox11* deletion leads to decreased post-mitotic neurons (Chen *et al*, 2015). Combined phenotypes from loss of *Sox4/11* thus resemble the neurogenesis defects observed in DKO embryos. Mouse *Sox4* contains a putative GSK3 phosphorylation site consisting of three serines spaced by three amino acids (SxxSSxxSS(316)P) (Fig 4A), a common feature of GSK3 motifs (Beurel *et al*, 2015). Mouse *Sox11* contains two putative GSK3 phosphorylation sites: (S(244)PxxS)

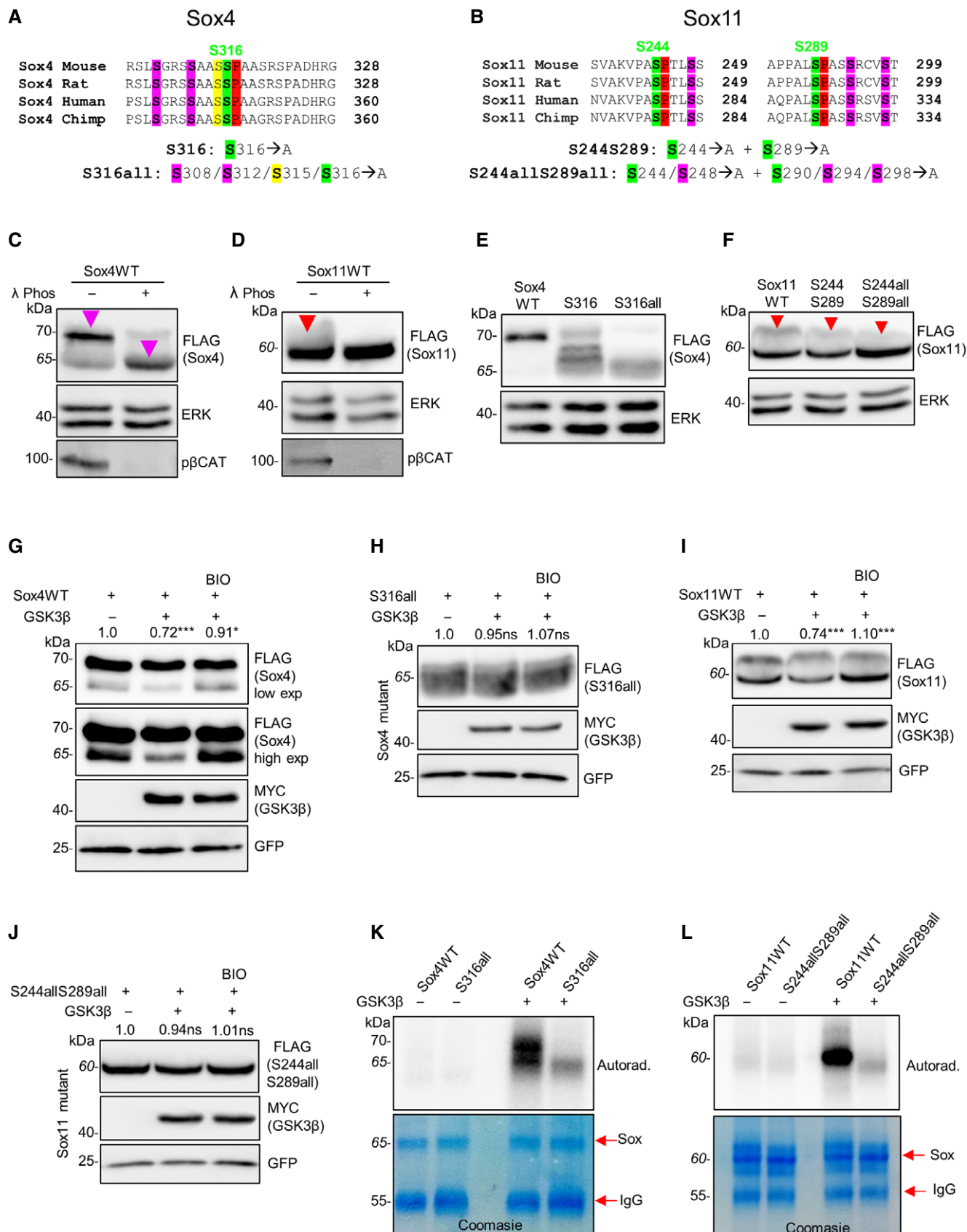


Figure 4.

Figure 4. Sox4/11 are direct GSK3 targets.

- A Amino acid sequence alignment of Sox4 GSK3 phospho-motif from mouse, rat, human and chimp. Mouse serine 316 (S316) (highlighted in green) and S315 (highlighted in yellow) predicted by *PhosphoSitePlus* to be phosphorylated. For S316 mutant, serine 316 mutated to alanine and for S316all mutant all highlighted serines mutated to alanine. Red highlight indicates proline residue following mutated serine.
- B Amino acid sequence alignment of Sox11 GSK3 phospho-motifs from mouse, rat, human and chimp. Mouse S244 and S289 (highlighted in green) predicted by *PhosphoSitePlus* to be phosphorylated. For S244S289 mutant, serines 244 and 289 mutated to alanine and for S244allS289all mutant all highlighted serines mutated to alanine. Red highlights indicate proline residues following mutated serines.
- C Analysis of Flag-tagged Sox4 wild-type (WT) protein overexpressed in HEK293T (293T) cells and detected with FLAG antibody. Lysates were treated with or without lambda-phosphatase (λ -Phos). Antibody against phosphorylated β -catenin (β cat) was used to validate λ -Phos treatment. Purple arrowheads indicate Sox4 phospho-shift from 70 to 65 kDa. ERK blot shows similar loading of samples.
- D Analysis of Flag-tagged Sox11 WT protein overexpressed in 293T cells and detected with FLAG antibody. Lysates treated with or without λ -Phos. Upper smear (red arrowhead) represents phosphorylated Sox11. Antibody for β cat was used to validate λ -Phos treatment.
- E Analysis comparing molecular masses of WT Sox4 to S316 and S316all mutants. ERK blot shows similar loading of samples.
- F Analysis comparing molecular masses of WT Sox11 to S244S289 and S244allS289all mutants. Red arrowheads indicate downward shifts of phosphorylated Sox11. ERK blot shows similar loading of samples.
- G Co-transfection of myc-tagged *GSK3 β* and *Flag-Sox4* in 293T cells. BIO treatment (0.5 μ M) performed for 1 h prior to harvest. Lower band (65 kDa) represents non-phosphorylated Sox4. High and low exposure (exp) blots shown to better visualize non-phosphorylated Sox4. Numbers above blot are quantification of Sox4 protein levels normalized to GFP and are expressed as fold change vs. controls. The sum of upper and lower bands was quantified ($n = 8$ biological replicates).
- H *Myc-GSK3 β* and S316all mutant co-transfection in 293T cells plus 0.5 μ M BIO treatment 1 h prior to harvest. Protein levels quantified as in (G) ($n = 4$ biological replicates).
- I *Myc-GSK3 β* and *Flag-Sox11* co-transfection in 293T cells. BIO treatment (0.5 μ M) performed for 1 h prior to harvest. Upper band represents phosphorylated Sox11. Numbers above blot are quantification of Sox11 protein levels normalized to GFP and are expressed as fold change vs. controls. The sum of lower and upper bands was quantified ($n = 14$, experiment performed 4 \times in triplicate and once in duplicate).
- J *Myc-GSK3 β* and S244allS289all mutant co-transfection in 293T cells plus 0.5 μ M BIO treatment 1 h prior to harvest. Protein levels quantified as in (I) ($n = 6$, experiment performed 2 \times in triplicate).
- K *In vitro* kinase assay on immunopurified Sox4WT and S316all mutant using recombinant GSK3 β protein and radiolabelled ATP. Samples were treated with λ -Phos prior to assay and run on Phos-tag gel. Coomassie Blue staining shows equal loading of WT and mutant proteins.
- L *In vitro* kinase assay of purified Sox11WT and S244allS289all mutant using recombinant GSK3 β protein and radiolabelled ATP. Experiment performed as in (K).

Data information: (C–J) Immunoblot analyses. Protein ladder numbers in italics indicate estimated size. Unpaired two-tailed *t*-test for all statistical analyses: ns, not significant; * $P < 0.05$, *** $P < 0.001$. $P = 0.00010$ (G, 2nd lane); $P = 0.049$ (G, 3rd lane); $P = 0.76$ (H, 2nd lane); $P = 0.83$ (H, 3rd lane); $P = 0.00030$ (I, 2nd lane); $P = 0.00020$ (I, 3rd lane); $P = 0.36$ (J, 2nd lane); $P = 0.67$ (J, 3rd lane).

Source data are available online for this figure.

and (S(289)PxxSxxxS) (Fig 4B). The Sox4/11 GSK3 sites are highly conserved in other mammals such as chimps and humans. Moreover, S315 and S316 of the Sox4 motif, and S244 and S289 of the Sox11 motifs, are phosphorylated according to *PhosphoSitePlus* (Hornbeck *et al*, 2012) (Fig 4A and B). Sox11 S244 and S289 phosphorylation was also reported elsewhere (Balta *et al*, 2018a). Finally, *in silico* analysis by NetPhos 3.1 (Blom *et al*, 1999) predicted GSK3 to be a top candidate for phosphorylating S316 of the Sox4 motif and both S244 and S289 of the Sox11 motifs (Fig 4A and B).

To determine whether Sox4/11 are indeed phosphorylated, we overexpressed N-terminally Flag-tagged *Sox4/11* in HEK293T (293T) cells and treated protein lysates with λ -phosphatase. Immunoblot analysis revealed a downshift of Sox4 from 70 to 65 kDa (Fig 4C), and a downshift of a higher molecular weight smear representing phosphorylated Sox11 (Fig 4D). Endogenous Sox4 was also downshifted upon λ -phosphatase treatment (Fig EV4A). By IF, overexpressed Sox4/11 mainly localized to the nucleus with only minor cytoplasmic staining, consistent with their role as transcription factors, validating our constructs (Fig EV4B and C). Next, we tested the effects of mutating the potential GSK3 phospho-motifs of Sox4/11. For Sox4, we generated a mutant in which only S316 was mutated to alanine and one in which all five serines were mutated (S316all) (Fig 4A). For Sox11, we generated a mutant in which S244 and S289 were mutated (S244S289) and one where all serines of both motifs were mutated (S244allS289all) (Fig 4B). Immunoblot analysis revealed a downshift in the Sox4 S316 mutant, with multiple bands migrating lower than the expected size of wild-type Sox4.

The S316all mutant revealed an even more drastic downshift, mimicking the effect of phosphatase treatment on wild-type Sox4 (Fig 4E). For Sox11, a minor downward shift of phosphorylated Sox11 was detected in the S244S289 mutant, while a more obvious shift was detected in S244allS289all mutants, with concomitant increase in the major Sox11 band, corresponding to unphosphorylated Sox11 (Fig 4F).

Next, we tested the effect of GSK3 β overexpression on Flag-Sox4/11 by co-transfection in 293T cells. GSK3 β overexpression led to a slight but significant decrease in total Sox4 protein levels, with a greater decrease observed in non-phosphorylated Sox4 (65 kDa band) (Fig 4G). Importantly, this effect was reversed by 1-h treatment with the GSK3 inhibitor 6-bromoindirubin-3'-oxime (BIO) (Fig 4G). GSK3 β overexpression and BIO treatment had no effect on the S316all mutant form of Sox4, confirming this site is a GSK β phospho-motif (Fig 4H). GSK3 β overexpression also reduced Sox11 protein levels, especially in non-phosphorylated Sox11, and this effect was reversed by 1 h BIO treatment (Fig 4I). GSK3 β overexpression and BIO treatment had no effect on the S244allS289all mutant form of Sox11 (Fig 4J).

To test whether Sox4/11 are directly phosphorylated by GSK3, we immunopurified wild-type and mutant (S316all and S244allS289all) Sox4 and Sox11, treated the proteins with λ -phosphatase and then performed *in vitro* kinase assays by incubating with recombinant GSK3 β and gamma-³²P-labelled ATP. Wild-type Sox4/11 were both highly phosphorylated by GSK3 β , while only minimal phosphorylation of the corresponding mutants could be detected (Fig 4K and L). Because WNT/STOP signalling inhibits

GSK3 β to protect target proteins from proteasomal degradation (Taelman *et al*, 2010; Acebron *et al*, 2014), we tested whether Sox4/11 are ubiquitinated by co-transfecting HA-tagged ubiquitin with *Flag-Sox4/11* and then briefly treating with MG132 to block proteasomal degradation of ubiquitin-conjugated polypeptides. Pull-down of Sox proteins with FLAG followed by immunoblot against HA-ubiquitin revealed a characteristic polyubiquitin-smear in both *Sox4* and *Sox11*-transfected cells, indicating that both Sox proteins are ubiquitin-conjugated (Fig EV4D and E). We conclude that Sox4/11 are (i) directly phosphorylated by GSK3 β and (ii) regulated by proteasomal degradation.

Sox4/11 protein levels are decreased in DKO NPCs, predominantly during mitosis

We next tested whether Sox4/11 are regulated by GSK3 in NPCs, focusing first on Sox4. We treated cultured NPCs with BIO for 24 h and analysed endogenous Sox4 protein levels by immunoblot analysis. BIO treatment led to an overall increase in Sox4, with an even greater increase in the lower, non-phosphorylated band (Fig EV5A). Importantly, mutant *Ccny/11* NPCs showed significantly reduced Sox4 protein levels (Fig 5A), even though *Sox4* mRNA levels were slightly elevated (Fig EV5B). We next analysed Sox4 protein levels in the neocortex of E13.5 embryos *in vivo*. By IF, Sox4 co-localized with *Ccny* and pLRP6 (S1490) in the SVZ (Fig EV5C), and was concentrated in mitotic BPs (Fig EV5D). In APs, Sox4 was enriched at mitosis (Fig EV5D). In DKO embryos, we could not detect an obvious decrease in Sox4 staining intensity in *Tbr2*⁺ cells (Fig EV5E). Likewise, immunoblot analysis of DKO forebrain lysates showed no reduction in total Sox4 protein levels (Fig EV5F), and qPCR analysis of RNA extracted from dorsal forebrains revealed no significant changes in *Sox4* expression ($P = 0.87$; Fig EV5G). In contrast, focusing on mitotic (pHH3⁺) BPs by IF, Sox4 protein levels were greatly reduced in DKO neocortex (-42% , $P = 0.0002$; Fig 5B and C). To further investigate WNT/STOP regulation of Sox4 during mitosis, we treated NPC cultures with nocodazole to arrest cells in G2/M. Interestingly, nocodazole-treated mutant NPCs displayed a greater reduction of Sox4 compared to non-treated cells (-45% , $P = 0.02$ vs. -25% , $P = 0.001$) (Fig EV5H). G2/M arrest by nocodazole treatment was validated by FACS analysis of NPCs (Fig EV5I).

To further investigate Sox4 regulation in NPCs, we raised a phospho-specific antibody targeting the S316 site of Sox4 (pSox4) (Fig 5D, schematic). Immunoblot analysis of overexpressed *Flag-Sox4* in 293T cell lysates treated with λ -phosphatase revealed a specific band at 70 kDa in the non-treated samples only, demonstrating specificity of the antibody towards phosphorylated Sox4 (Fig EV5J). The pSox4 antibody did not detect the S316 mutant upon immunoblotting (Fig EV5K). Treatment of *Flag-Sox4*-transfected 293T cells with BIO led to decreased Sox4 phosphorylation, and this effect was greater in nocodazole-treated cells (Fig 5E). Moreover, immunoblot analysis of forebrains revealed a specific band at 70 kDa, representing phosphorylated Sox4, that was increased in DKO embryos (Fig 5F), consistent with elevated phosphorylation by GSK3.

For Sox11, *Ccny/11* mutant NPCs revealed strongly reduced protein levels and elevated (not significant) mRNA levels, similar to Sox4 (Figs 5G and EV5L). Moreover, IF analysis on E13.5 neocortex sections revealed significantly decreased Sox11 protein levels in

mitotic cells within the SVZ (-23% , $P = 0.04$) (Fig 5H and I). Sox11 protein levels were also decreased in newborn neurons and non-mitotic BPs, as evidenced by immunoblot analysis of forebrain protein lysates and co-IF with *Tbr2* (-10% , $P = 0.01$), respectively (Fig 5J–L). Expression of *Sox11* was not significantly altered in DKO dorsal forebrains ($P = 0.46$), confirming the regulation of Sox11 by *Ccny/11* is post-transcriptional (Fig EV5M). Finally, Sox11 co-localized with *Ccny* and pLRP6 in the SVZ (Fig EV5N). In summary, *Ccny/11* deficiency leads to decreased Sox4/11 protein levels in NPCs and predominantly in mitotic cells, consistent with Sox4/11 being novel WNT/STOP targets in the developing neocortex.

Sox4/11 overexpression and GSK3 inhibition both rescue differentiation defects of DKO NPCs

To test whether Sox4/11 misregulation accounts for the decreased cortical neurogenesis observed in DKO embryos, we attempted to rescue the neurogenesis defect in mutant NPCs by overexpressing both proteins using lentiviral transduction of *Flag-Sox4* and *Flag-Sox11* in the pLenti-CAG-IRES-EGFP vector (Fig 6A, schematic). To avoid possible toxic effects resulting from excessive viral load, we isolated NPCs from DKO and control (*Ccny*^{+/−}/*Ccny11*^{+/−}) E13.5 neocortex instead of performing shRNA knockdown of *Ccny*. DKO NPCs exhibited similar neurogenesis defects as sh*Ccny*-treated *Ccny11* mutants, showing reduced *Tuj1* staining (Fig 6B and C). For rescue experiments, we transduced DKO and control NPCs with *Sox4* and *Sox11*-overexpressing lentiviruses, or empty pLenti-CAG-IRES-EGFP vector lentivirus as a control, incubated the cultures in differentiation medium, and then monitored neuronal output by IF for *Tuj1* and *Map2* (microtubule-associated protein 2, an additional neuron marker). IF for GFP or FLAG was used to identify NPCs infected with control or *Sox4/11* lentiviruses, respectively. Overexpression of *Sox4/11* was monitored by qPCR and IF, which revealed, respectively, increased *Sox4/11* mRNA levels and high transduction efficiency in NPCs (Appendix Fig S2A–F). Strikingly, *Sox4/11* overexpression in DKO NPCs led to an almost complete rescue in the number of *Tuj1*⁺ and *Map2*⁺ cells generated when compared to DKO NPCs transduced with empty vector (Fig 6B and C; Appendix Fig S3A and B). Importantly, control cells transduced with *Sox4/11* lentiviruses showed no significant increase in the number of newly formed *Tuj1*⁺/*Map2*⁺ neurons (Fig 6B and C; Appendix Fig S3A and B). Interestingly, many of the rescued *Tuj1*⁺/*Map2*⁺ cells lacked mature neurites (Fig 6B, asterisks; Appendix Fig S3A, asterisks; quantified in Appendix Fig S3C), suggesting that *Sox4/11* overexpression can rescue initial stages of neurogenesis but not full neuronal differentiation in DKO NPCs.

Finally, to corroborate that the DKO differentiation phenotype in cultured NPCs is indeed due to diminished WNT signalling, we carried out a rescue experiment. We treated control and DKO NPCs with the GSK3 inhibitor CHIR99021 (CHIR) and monitored neuronal output by IF for *Tuj1* (Fig 6D, schematic). Strikingly, 1 μ m CHIR treatment in DKO NPCs led to a significant increase in the number of, mostly, immature neurons, while 3 μ m CHIR treatment restored the level of mature neurons to that of controls, thereby leading to a complete rescue (Fig 6E and F). CHIR treatment also promoted neurogenesis in control NPCs, which is consistent with previous reports (Rosenbloom *et al*, 2020), and however, the increase in neurogenesis observed was significantly lower when compared to

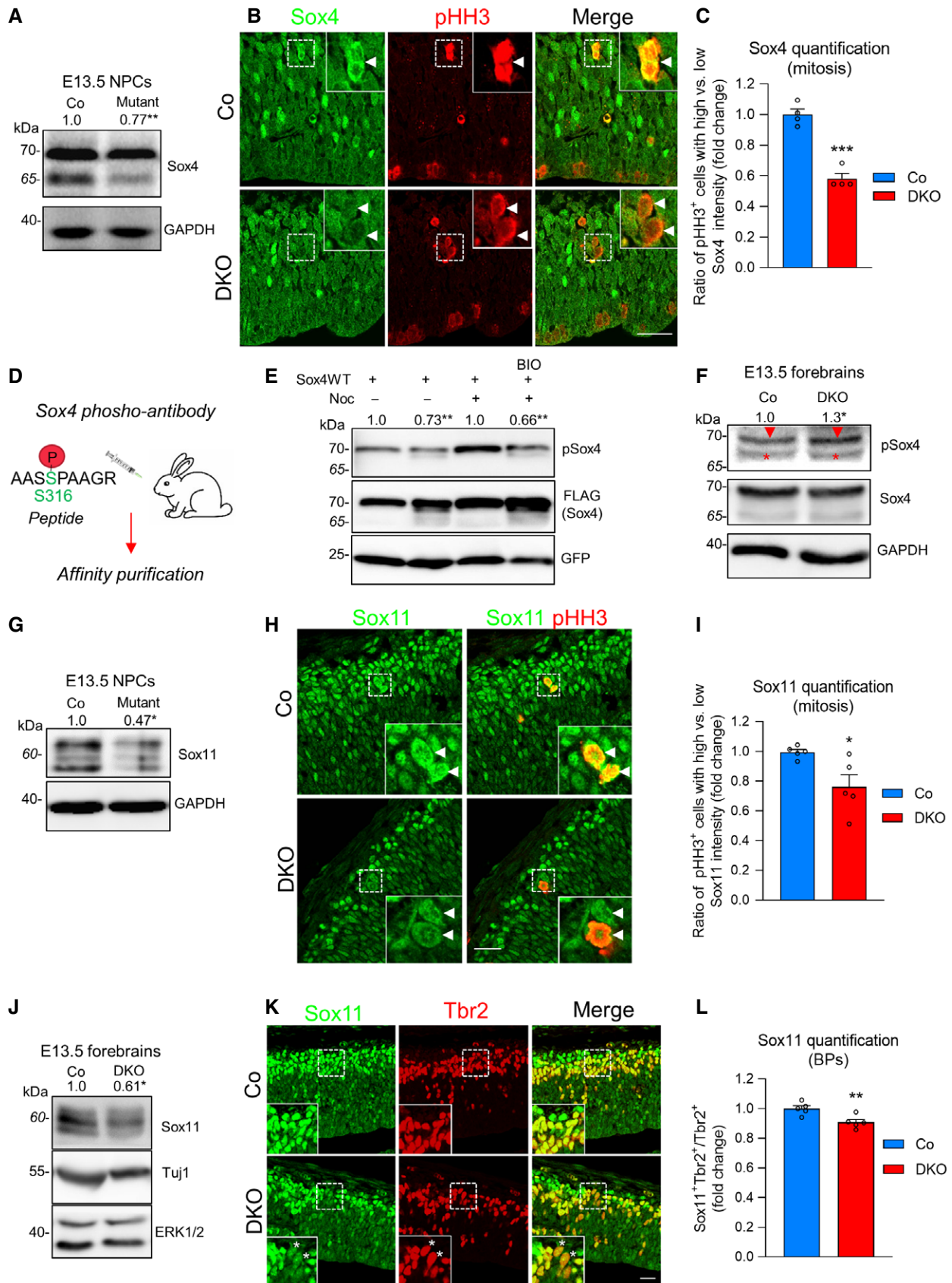


Figure 5.

Figure 5. Sox4/11 protein levels are decreased in DKO NPCs, predominantly during mitosis.

- A Immunoblot analysis with Sox4 antibody of protein lysates extracted from control (Co) (*Ccny*^{+/-}; *Ccny1*^{-/-}; shRNA Co) and mutant (*Ccny*^{+/-}; *Ccny1*^{-/-}; shRNA *Ccny*) NPCs. Numbers are fold change vs. controls of Sox4 protein levels normalized to GAPDH (*n* = 3). Immunoblot image cropped from Fig EV5H. Quantification performed on immunoblot shown in Fig EV5H and two additional immunoblots (not shown).
- B IF for Sox4 and pHH3 on neocortex sections of E13.5 control and DKO embryos. The level of Sox4 immunoreactivity is reduced in pHH3⁺ cells (white arrowheads).
- C Quantification of Sox4 staining in SVZ mitotic cells from E13.5 control and DKO embryos. Mitotic Sox4 staining was defined as high if the pixel intensity was similar to, or higher than, non-mitotic cells, or low if the levels were below those observed in non-mitotic cells. Data are means ± SEM for ratios of cells with high vs. low Sox4, and are displayed as fold change vs. controls (*n* = 4 embryos, 3 litters).
- D Strategy to generate Sox4 S316 phospho-antibody (pSox4) by phosphopeptide injection into rabbits.
- E *Flag-Sox4* transfection in 293T cells followed by 24-h nocodazole (100 ng/ml) and BIO (1 μM) treatments. Samples analysed by immunoblot using pSox4 antibody; numbers above blot are quantification of Sox4 phospho-band normalized to total Sox4 (FLAG) for nocodazole-treated and non-treated cells and are expressed as fold change vs. controls (*n* = 6, experiment performed 2× in triplicate).
- F Immunoblot analysis with pSox4 antibody of cell lysates extracted from E13.5 control and DKO forebrains. Red arrowheads indicate Sox4 phosphorylation band; red asterisks are non-specific bands. Numbers above blot are quantification of Sox4 phosphorylation levels normalized to total Sox4 and are expressed as fold change vs. controls (*n* = 4 embryos, 3 litters).
- G Immunoblot analysis with a Sox11 antibody of protein lysates extracted from control and mutant E13.5 NPCs. Numbers are fold change vs. controls of Sox11 protein levels normalized to GAPDH (*n* = 3 biological replicates).
- H IF for Sox11 and pHH3 in E13.5 control and DKO neocortices. Sox11 staining intensity is decreased in mitotic cells (white arrowheads, insets).
- I Quantification of Sox11 protein levels in SVZ mitotic cells from E13.5 control and DKO embryos. Quantification performed as in (C). Data are means ± SEM for ratios of high vs. low Sox11 and are displayed as fold change vs. controls (*n* = 5 embryos, 3 litters).
- J Immunoblot analysis with a Sox11 antibody of protein lysates extracted from E13.5 control and DKO forebrains. Numbers are fold change vs. controls of Sox11 protein levels normalized to Tuj1 (*n* = 5 embryos, 4 litters). ERK1/2 immunoblot shown to document equal loading.
- K Co-IF for Sox11 and Tbr2 in sections of neocortex of E13.5 control and DKO embryos. Sox11 immunoreactivity is reduced in some Tbr2⁺ cells (asterisks, insets).
- L Quantification of percentage of Tbr2⁺ cells that show with high Sox11 staining intensity, in control and DKO E13.5 neocortices. High or low staining intensity was judged based on visual inspection, taking background staining levels into account. Data are means ± SEM and are shown as fold change vs. controls (*n* = 5 embryos, 3 litters).

Data information: All scale bars 20 μm. Protein ladder numbers in italics indicate estimated size. Unpaired two-tailed t-test for all statistical analyses: ns, not significant; **P* < 0.05, ***P* < 0.01, ****P* < 0.001. *P* = 0.0012 (A); *P* = 0.00020 (C); *P* = 0.0031 (E, 2nd lane); *P* = 0.0010 (E, 4th lane); *P* = 0.047 (F, 2nd lane); *P* = 0.047 (G); *P* = 0.045 (I); *P* = 0.031 (J); *P* = 0.0010 (L).

Source data are available online for this figure.

CHIR-treated DKO NPCs (Fig 6F). Hence, we conclude that *Ccny*/*11* promote differentiation of cultured NPCs through the WNT signalling pathway.

Discussion

We set out to determine the role of WNT/STOP signalling in neocortex development by analysing mice mutant for *Ccny* and *Ccny1*, key regulators of the pathway. We find that WNT/STOP orchestrates the process of neurogenesis by (i) regulating symmetric vs. asymmetric AP division; (ii) controlling the length of the cell cycle, notably of mitosis, of BPs; and (iii) promoting neuron generation through Sox4 and Sox11 stabilization in BPs. The results suggest that WNT/STOP rather than WNT/β-catenin signalling is the primary driver of cortical neurogenesis. Our study reconciles seemingly contradictory reports by revealing a division of labour in neocortex development, whereby WNT/STOP promotes a differentiative process, i.e. the generation of NPCs committed to neurogenesis, whereas WNT/β-catenin predominantly promotes NPC self-renewal.

A division of labour between WNT/STOP and WNT/β-catenin signalling during neocortical neurogenesis

The precise biological role and molecular function of WNT signalling in the mouse neocortex has remained controversial. Most *in vivo* studies suggest that the primary role of canonical WNT signalling is to promote self-renewal at the expense of differentiation. This is particularly evident in β-catenin mutant mice, which display increased AP cell cycle exit and premature neurogenesis

(Mutch *et al*, 2010; Draganova *et al*, 2015). Although some studies have shown that β-catenin can also promote neuronal differentiation of NPCs (Hirabayashi *et al*, 2004; Israsena *et al*, 2004; Kuwahara *et al*, 2010), these studies were mostly performed *in vitro*, and are not supported by *in vivo* evidence. More recently, electroporation of Wnt3a into the neocortex of developing mouse embryos increased both, proliferation of APs and differentiation of BPs, seemingly resolving the controversy and leading the authors to conclude that canonical WNT can indeed promote both processes in a cell type-specific manner (Munji *et al*, 2011). However, this study relied on manipulating WNT signalling at the ligand level, which not only affects WNT/β-catenin but also WNT/STOP signalling, which was not examined. WNT/STOP acts through the same WNT/LRP6/GSK3 axis but bifurcates upstream- and is independent of β-catenin. Its primary output is not transcription but post-transcriptional protein stabilization (Acebron & Niehrs, 2016).

We now propose a new model (Fig 6D), whereby WNT/STOP promotes neuron generation from BPs through stabilization of Sox4/11 while canonical WNT/β-catenin signalling promotes AP self-renewal. Our conclusions based on the analysis of E13.5 DKO embryos are further supported by the results of *Ccny*/*11* knockdown at later stages of neocortex development *in vivo* and of NPC culture experiments *in vitro*. Together, these data show reduced generation of BPs, and consequently of neurons, in the absence of *Ccny*/*11*. We therefore conclude that DKO embryos exhibit reduced neurogenesis through decreased generation of BPs from APs and of post-mitotic neurons from BPs. However, while our data demonstrate that the knockout of *Ccny*/*11* does not affect WNT/β-catenin signalling, they do not rule out the possibility that WNT/β-catenin signalling can also contribute to these processes.

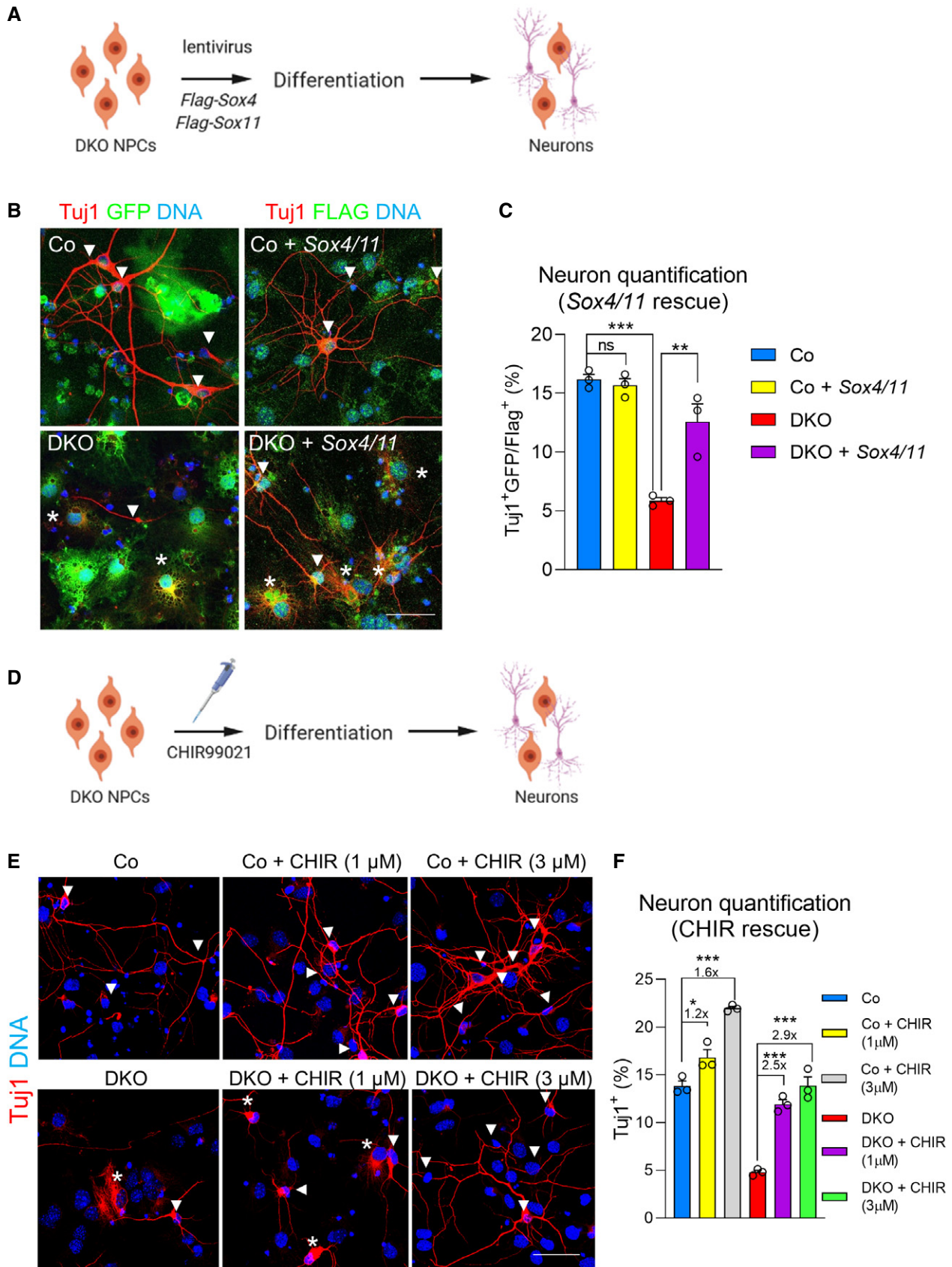


Figure 6.

Figure 6. Sox4/11 overexpression and GSK3 inhibition both rescue differentiation defects of DKO NPCs.

- A Schematic illustrating strategy to rescue DKO NPC differentiation defect by simultaneous lentiviral overexpression of *Flag-Sox4* and *Flag-Sox11* with two lentiviruses. Created with Biorender.com.
- B IF for Tuj1 and Map2 (not shown) to identify newly formed neurons in NPCs after seven-day culture in differentiation medium. Empty CAG-IRES-EGFP vector was used as control in cells not transduced with *Sox4/11*. Transduced cells were identified by IF for GFP (Co and DKO) or FLAG (Co + *Sox4/11* and DKO + *Sox4/11*). Arrowheads indicate mature neurons, and asterisks denote immature neurons lacking neurite extension. Scale bar 20 μ m.
- C Quantification of transduced Tuj1⁺ cells from (B). Note the decrease in neuron number in DKO cultures compared to control, and the rescue in DKO cultures upon *Sox4/11* expression (experiment performed twice in triplicates, representative experiment shown). Data are means \pm SEM.
- D Schematic illustrating the rescue DKO NPC differentiation defect with the GSK3 inhibitor CHIR99021 (chemical name: 6-[2-[[4-(2,4-dichlorophenyl)-5-(5-methyl-1H-imidazol-2-yl)pyrimidin-2-yl]amino]ethylamino]pyridine-3-carbonitrile). Created with Biorender.com.
- E IF for Tuj1 to identify newly formed neurons in NPCs after seven-day culture in differentiation medium. Arrowheads indicate mature neurons, and asterisks denote immature neurons lacking neurite extension. Scale bar 20 μ m.
- F Quantification of Tuj1⁺ cells in control, control + CHIR (1 μ M, 3 μ M), DKO, and DKO + CHIR NPC cultures. Data are means \pm SEM (experiment performed twice in triplicates, representative experiment is shown). Numbers below asterisks show fold change.

Data information: One-way ANOVA test for all statistical analyses: ns, not significant; * $P < 0.05$, ** $P < 0.01$, *** $P < 0.001$. $P = 0.97$ (C, yellow bar); $P = 0.00010$ (C, red bar); $P = 0.0023$ (C, purple bar); $P = 0.031$ (F, yellow bar); $P = 5 \times 10^{-6}$ (F, grey bar); $P = 2 \times 10^{-5}$ (F, purple bar); and $P = 1 \times 10^{-6}$ (F, green bar). Source data are available online for this figure.

LRP6 is a key regulator in WNT/STOP and its phosphorylation at G2/M by the Cnny/CDK complex leads to GSK3 inhibition and activation of the pathway notably during mitosis, when transcription is low (Davidson *et al*, 2009). Interestingly, analysis of *Lrp6* mutant mice reveals a thinner neocortex, reduced neuronal differentiation, and only minor changes in proliferation (Zhou *et al*, 2006). Similarly, deficiency in *actin-binding protein filamin A* induces neurogenesis defects within the mouse cerebral cortex and impairs LRP6/GSK3 signalling and asymmetric cell division (Lian *et al*, 2016; Lian *et al*, 2019). These phenotypes are remarkably similar to those observed here in *Cnny/11* DKO embryos, suggesting that *Lrp6* mutants primarily present a WNT/STOP signalling defect. The reason why *Lrp6* mutants do not also manifest the proliferation defects of β -catenin mutants is unclear, but may be due to compensation from LRP5. Functional redundancy between LRP5 and LRP6 in WNT/ β -catenin signalling is well documented (Kelly *et al*, 2004; Goel *et al*, 2012; Zhong *et al*, 2012; Liu *et al*, 2019).

WNT/STOP signalling promotes neurogenesis via Sox4 and Sox11 stabilization

An important finding of this study is the identification of the neurogenic transcription factors Sox4 and Sox11 as *bona fide* WNT/STOP targets. Several links between SoxC transcription factors and WNT signalling are known: Sox4 and Sox11 interact with the β -catenin destruction complex and, in lung cancer cells, Sox4 is a direct target of β -catenin (Bhattaram *et al*, 2014; Melnik *et al*, 2018). Our data support and further develop these links by showing that Sox4/11 are directly phosphorylated by GSK3 and thereby targeted for proteasomal degradation. We also show that the majority of Sox4 is phosphorylated at a single GSK3 phosphomotif, while Sox11 contains two motifs and is only partially phosphorylated. GSK3 phosphorylation is known to create phosphodegrons for recognition by E3 ubiquitin ligases leading to proteasomal degradation (Taelman *et al*, 2010). Consistent with this possibility, phosphorylation by GSK3 β induced ubiquitination and decreased overall Sox4 and Sox11 levels. Previous reports have shown that, in the neocortex, Sox11 cellular localization and protein stabilization are regulated by phosphorylation and ubiquitination, respectively, supporting that post-transcriptional regulation

of Sox11 is essential for its function *in vivo* (Balta *et al*, 2018a; Balta *et al*, 2018b; Chiang *et al*, 2021).

WNT/STOP mediated inhibition of GSK3 predominantly occurs in G2/M (Acebron *et al*, 2014). Consistently, we find that the stabilization of Sox4/11 by WNT/STOP is cell cycle-dependent, with peak levels in mitotic cells. WNT/STOP signalling in G2/M of mother cells is thought to endow daughter cells with a growth advantage, by stabilizing bulk protein. Deficiency in WNT/STOP signalling reduces G1 growth and delays cell cycle progression (Acebron *et al*, 2014; Huang *et al*, 2015). Analogously, WNT/STOP signalling in G2/M of NPCs may promote differentiation of daughter cells via elevated levels of Sox4/11 during G1/S-phase. An attractive hypothesis is that Sox4/11 are bookmarking transcription factors, that remain bound to chromosomes in mitosis to enable target gene reactivation in a timely fashion upon mitotic exit (Palozola *et al*, 2019).

The importance of decreased Sox4/11 protein levels for the neurogenesis defect of DKO embryos is highlighted by the fact that their overexpression can rescue the differentiation phenotype. Interestingly, the rescue is incomplete: Sox4/11 increase the number of Tuj1⁺ cells in differentiating DKO NPCs, but only partially restore their morphology, leading to immature neurons. The incomplete rescue may be due to unphysiologically high levels of Sox4/11 from lentiviral transduction since Sox11 overexpression inhibits dendritic morphogenesis (Hoshiba *et al*, 2016). Alternatively, WNT/STOP signalling may have additional targets required for neuronal maturation and morphogenesis. Indeed, proteomic analysis indicates hundreds of potential WNT/STOP target proteins in HeLa cells (Acebron *et al*, 2014).

WNT/STOP signalling promotes asymmetric AP division

Another important insight of this work is that *Cnny/11* are required to promote asymmetric division of APs, which is in keeping with their physiological role as the starting point of cortical neurogenesis, since more asymmetric AP divisions lead to more BPs and hence post-mitotic neurons. In *C. elegans* embryos, WNT signalling is long known to regulate spindle asymmetry (Sugioka *et al*, 2011), and in embryonic stem cells, a Wnt3a point source can polarise the mitotic spindle to give rise to asymmetric cell division (Habib *et al*, 2013).

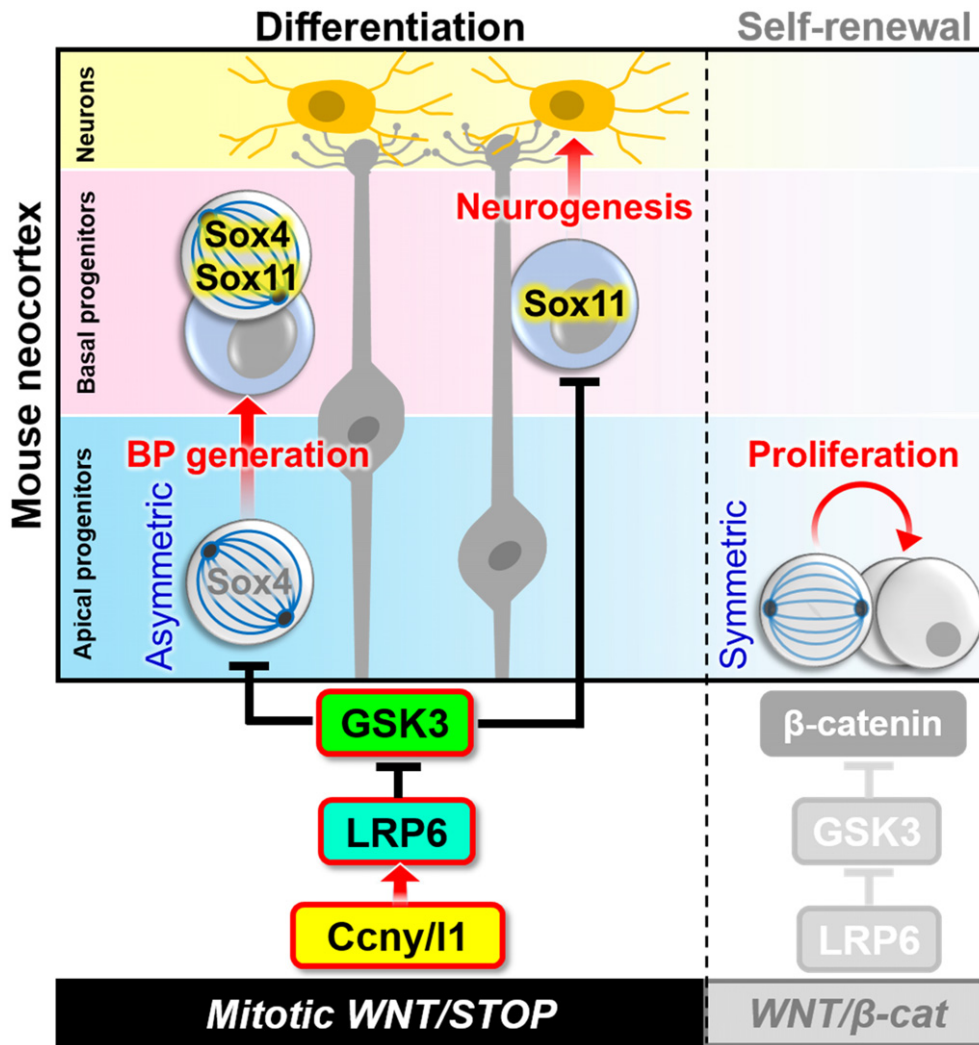


Figure 7. Division of labour model between WNT/STOP and WNT/β-catenin signalling during neocortical neurogenesis.

Ccny/I1 stimulate cyclin-dependent kinases (CDK) 14 and 16 predominantly during G2/M (not shown) to phosphorylate and activate LRP6. This co-receptor activation leads to a peak of WNT/STOP signalling and GSK3 inhibition in mitosis. Mitotic WNT signalling has two consequences: First, it increases asymmetric AP division via unknown effectors, which leads to more basal progenitors and hence post-mitotic neurons; second, it protects Sox proteins from proteasomal degradation. Sox4 stabilization in mitotic APs leads to increased BP generation, and its stabilization in mitotic BPs may promote BP self-renewal and/or differentiation. Sox11 is stabilized in both mitotic and non-mitotic cells of the SVZ, which leads to increased post-mitotic neuron generation. WNT/β-catenin signalling primarily promotes AP self-renewal.

Taken together, these studies support that WNT/STOP signalling promotes asymmetric AP division.

Although we have not identified the molecular targets responsible for the decreased asymmetric AP division in DKO embryos, we narrowed down the mechanism to an increase in apical-basal aMTs, which can directly stabilize the positioning of the mitotic spindle and thus promote symmetric AP division (Mora-Bermúdez *et al*, 2014). This finding is consistent with recent work in which GSK3 overexpression and inhibition of WNT secretion in HCT116 cells increase MT polymerization rates during mitosis (Lin *et al*, 2020). Interestingly, WNT/STOP inhibition has been also shown to induce mitotic spindle defects and improper chromosome segregation (Stolz *et al*, 2015; Lin *et al*, 2020), pointing towards a more general role of WNT/STOP signalling in promoting mitotic spindle assembly. One possibility is that WNT/STOP signalling modulates MT

plus ends, which are key determinants for spindle orientation (Lu & Johnston, 2013). Misregulation of MT plus ends may also explain the lengthened mitosis observed in DKO BPs. A candidate WNT/STOP target protein is Kif2a (Taelman *et al*, 2010), a MT plus end regulator that is required for cortical neurogenesis (Sun *et al*, 2017; Ding *et al*, 2019). On the other hand, we cannot exclude cross-talk between WNT/STOP and the WNT/PCP-pathway, which is also implicated in asymmetric division in cortical progenitors (Delaunay *et al*, 2014).

Mitosis is a critical time window for determining NPC fate

Our study suggests that β-catenin-independent WNT signalling impacts neurogenesis preferentially during mitosis: (i) LRP6 is maximally phosphorylated and activated in mitotic NPCs, (ii) Sox4/11

protein levels peak in mitotic NPCs, (iii) apical-basal aMTs and symmetric cell division are both increased in DKO APs, and (iv) mitosis is retarded in BPs. These observations are consistent with the facts that WNT/STOP signalling stabilizes proteins specifically in mitosis (Acebron *et al*, 2014) and regulates cell cycle progression of mitotic cells (Huang *et al*, 2015; Stolz *et al*, 2015). The process of neurogenesis is intricately connected to the cell cycle length of NPCs (Götz & Huttner, 2005; Dehay & Kennedy, 2007; Borrell & Calegari, 2014). Thus, lengthening the cell cycle of APs induces premature neurogenesis (Calegari & Huttner, 2003). Conversely, shortening the cell cycle of APs by reducing G1 delays neurogenesis and promotes generation and expansion of BPs (Lange, *et al*, 2009). It is unclear at which point in the cell cycle NPCs commit to neuronal differentiation. However, given that *Ccny/11* deficiency reduces neuronal output and that the regulation of neurogenesis by WNT/STOP occurs primarily during cell division, we conclude that mitosis represents a key phase of the cell cycle when NPCs commit to a neurogenic fate. This conclusion reverberates the observation that many human microcephaly associated genes encode mitotic regulators (Hu *et al*, 2014).

In summary, our findings resolve the controversy regarding the role of WNT signalling in neocortex development by demonstrating that WNT/STOP is the primary driver of a differentiative process *in vivo*, i.e. the generation of neurons from NPCs, whereas WNT/ β -catenin promotes NPC self-renewal. They also emphasize the importance of mitosis as a critical determinant of NPC fate, when asymmetric AP division and Sox4/11 protein stabilization in BPs are orchestrated by post-transcriptional WNT signalling.

Materials and Methods

Animals

Mice were bred in the Central Animal Laboratory in the DKFZ, Heidelberg, under standardized hygienic conditions. All animal work was conducted according to national and international guidelines and was approved by the state review board of Baden-Württemberg (protocol no. G-123/18). Sperm from mice carrying a flanked by loxP (floxed) allele of cyclin Y (*Ccny*^{tm1(flox)Smoc}) was obtained from the lab of Ariel Zeng (Shanghai, China; An *et al*, 2015) and used for *in vitro* fertilization of wild-type C57BL/6N oocytes. Heterozygous *Ccny*-flox mice were bred with transgenic animals expressing Cre recombinase under the control of the CMV promoter to achieve organism-wide gene knockout (*Ccny*KO). Generation of cyclin Y-like 1-deficient (*Ccny11tm1a*^{(EUCOMM)Wtsi}/H; *Ccny11*KO) mice has been described previously (Koch *et al*, 2015). *Ccny* and *Ccny11* double knockout embryos (DKO) were generated by incrossing *Ccny*^{-/-}*Ccny11*^{+/-} males with *Ccny*^{+/-}*Ccny11*^{-/-} females. *Ccny*^{+/-}; *Ccny11*^{+/-} embryos were used as controls. Embryos were analysed at various time points (E11.5, E12.5 and E13.5), and gender was not taken into consideration. For proliferation assays, BrdU (Sigma-Aldrich, B5002) and IdU (Sigma-Aldrich, I0050000) were dissolved in 0.9% NaCl and administered to pregnant dams via intraperitoneal (IP) injection at a dose of 50 mg/kg. Injection strategies are indicated in the figure legends. Adult mice were sacrificed by cervical dislocation.

For *in utero* electroporation experiments, C57BL/6J mice were bred at the Biomedical Services Facility of the MPI-CBG under standardized hygienic conditions and all procedures were conducted in agreement with the German Animal Welfare Legislation after approval by the Landesdirektion Sachsen (licenses: mouse TVV 5/2015 and TVV 20/2020).

In utero electroporation

Wild-type C57BL/6J pregnant mice carrying E13.5 embryos were anesthetized using initially 4% isoflurane (Baxter, HDG9623), followed by 2–3% isoflurane during the *in utero* electroporation (IUE) procedure. The animals were injected subcutaneously with the analgesic (0.1 ml of metamizol, 200 mg/kg). The peritoneal cavity was surgically opened and the uterus exposed. Using borosilicate microcapillary (Sutter instruments, BF120-69-10), the embryos were injected intraventricularly with a solution containing 0.1% Fast green (Sigma-Aldrich, F7252) in sterile PBS, 2 μ g/ μ l of pSuper plasmid (either 2 μ g/ μ l of pSuper-shcon or 1 μ g/ μ l of pSuper-shCny and 1 μ g/ μ l of pSuper-shCny11), 0.4 μ g/ μ l of pCAGGS GFP. The electroporations (six 50-msec pulses of 28V at 1 s intervals) were performed using a 3-mm diameter electrode (BTX genetronics Inc., 45-0052INT). After surgery, mice received Metamizol in drinking water (1.33 mg/ml).

Pregnant mice were sacrificed by cervical dislocation at the indicated time points (E15.5-E17.5), and embryonic brains were dissected, fixed in 4% PFA, overnight at 4°C and processed for cryosectioning.

Cell culture

HEK293T (293T) cells were cultured in DMEM (Gibco, 11960-044) supplemented with 10% v/v foetal bovine serum (Capricorn, FBS-12A9), 2 mM glutamine (Sigma-Aldrich, G7513) and 1% v/v penicillin/streptomycin (Sigma-Aldrich, P0781). Cells were grown at 37°C and 10% CO₂ in a humidified chamber. Transfections were performed using XtremeGENE 9 DNA transfection reagent (Roche, 06366244001) according to the manufacturer's instructions. Plasmids were transfected at either 200 ng/ml (*Flag-Sox4/Sox11*, GFP, HA-Ubiquitin) or 400 ng/ml (*Myc-GSK3 β*) in 24-well plates coated with poly-D-lysine (Sigma-Aldrich, P6407). Where indicated, cells were treated with bromindirubin-3'-oxime (BIO) (Cayman Chemical, 13123) or nocodazole (BioTrend, BN0389). Doses and duration of treatments are indicated in the figure legends. DMSO was used as a control for BIO and nocodazole treatments.

NPC isolation and culturing

NPCs were obtained by incrossing *Ccny*^{+/-} *Ccny11*^{+/-} animals and collecting embryos at E13.5. The forebrain cerebral cortex was dissected from individual embryos, dissociated into a single-cell suspension by repetitive pipetting and then filtered through a 70 μ m cell strainer (Corning, 431751). The resulting neurospheres were cultured in NPC media (DMEM/F12 (Invitrogen, p5780), B27 (LIFE, 1074547), glucose (Sigma-Aldrich, s5761) hepes, progesterone (Sigma-Aldrich, 12587010) putrescine (Sigma-Aldrich, p7556), heparin (Sigma-Aldrich, E4127) penicillin/streptomycin, insulin-transferrin-sodium selenite supplements (Roche, H3149), sodium

bicarbonate (Sigma-Aldrich, p5780) and 20 ng/ml EGF (Thermo Fisher, PHG0313) for 5–7 days before being passaged.

For passaging, cells were treated with accutase (Capricorn, ACC-1B) and then pipetted repetitively to obtain a single-cell suspension. Cells were passaged at least two times before performing experiments. Where indicated, NPCs were treated with BIO, CHIR99021 (Millipore, 361559), or nocodazole. Doses and duration of treatments are indicated in the figure legends.

For NPC differentiation assays, 2×10^5 /cells were plated on poly-D-lysine-coated 24-well plates for 48 h, and then, media was switched to NPC differentiation media (DMEM/F12, B27, glucose, hepes, progesterone, putrescine, heparin, penicillin/streptomycin, insulin–transferrin–sodium selenite supplements, and sodium bicarbonate). Cells were grown for 7–9 days to a confluency ~ 80% before being harvested for RNA, protein or IF analysis. Media was replaced every 48 h. Knockdown of *Ccny* was performed by transducing *shCcny* into NPCs 24 h prior to differentiation assays. For *Sox4/11* rescue experiments, *Flag-Sox4* and *Flag-Sox11*-overexpressing lentiviruses were transduced simultaneously into NPCs 24 h prior to differentiation assays. 4 µg/ml polybrene (Sigma-Aldrich, TR-1003) was added to media for all transductions. For rescue experiments by GSK3 inhibition, CHIR99021 was added to the differentiation media at the indicated concentrations for the entire duration of the differentiation protocol. DMSO was used as a control.

For FACS analysis, NPCs were fixed in 70% ethanol for 10 min, washed three times with PBS and then stained with 40 µg/ml propidium iodide (Thermo Fisher, BMS500PI) in FACS staining buffer (0.1% Triton X-100, 0.1% sodium citrate, in PBS) at 37°C for 30 min. Cells were then analysed according to Davidson *et al*, 2009 on a BD FACS Canto, and data were processed using FlowJo software.

Lentivirus preparation

The *Ccny* and *Ccny1* shRNA plasmids were obtained from the laboratory of Ariel Zeng and are described in Zeng *et al*, 2016. For the *Sox4* and *Sox11* overexpression plasmids, full-length *Flag-Sox4* and *Flag-Sox11* were excised from their respective pCS2⁺ plasmids (see below) and each ligated into the pLenti-CAG-IRES-EGFP plasmid using BamHI and BsrGI restriction sites to produce two separate lentiviruses. EGFP was removed with this cloning strategy for both the *Sox4*- and *Sox11*-overexpressing lentiviruses. All lentiviruses were packaged in 293T cells according to Lois *et al*, 2002.

Sox4/Sox11 cloning and mutagenesis

GoTaq (Promega, M7841) DNA polymerase was used to amplify full-length *Sox4* and *Sox11* using cDNA obtained from whole E13.5 embryos. N-terminal Flag tags were added via forward primers (see Appendix Table S1). BamHI and XhoI restriction sites were introduced by PCR to clone into the pCS2⁺ plasmid, and sequencing was performed to verify the integrity of the constructs. Mutagenesis of the *Sox4/11* GSK3 phospho-motifs was performed by amplifying full-length Flag-tagged plasmids with Phusion™ DNA polymerase (NEB, M0530L) using primers designed to mutate selected serines into alanines. Extension times of 5 min and 18 cycles were carried out for each PCR. Amplification products were PCR purified

(Machery Nagel, 740609.250), digested with DpnI restriction enzyme (NEB, R0176) for 1 h at 37°C, PCR purified again, and then transformed into electro-competent bacteria. Colonies were screened for mutations by sequencing. Double GSK3-motif mutations (e.g. for *Sox11*) were performed sequentially.

Real-time quantitative PCR

mRNA from NPCs and embryonic dorsal forebrains was extracted using the Nucleospin RNA XS kit (Machery-Nagel, 740902.50) and the Nucleospin RNA kit (Machery-Nagel, 740955.250), respectively, according to the manufacturer's instructions. Extracted mRNA was transcribed to cDNA using random hexamer primers. PCR was performed on a Roche Light Cycler 480 using the Universal ProbeLibrary system. *Gapdh* was used as a housekeeping gene unless otherwise stated. See Appendix Table S1 for primer sequences.

Immunoblotting

Cells were adjusted to equal numbers, washed with PBS, resuspended in triton lysis buffer (20 mM Tris-HCl, 150 M NaCl, 1% Triton X-100, 1 mM EDTA, 1 mM EGTA, 1 mM β-glycerolphosphate, 2.5 mM sodium pyrophosphate and 1 mM sodium orthovanadate), incubated for 30 min on ice and then spun down at full speed for 7 min to clear lysates. For brain tissue samples, forebrains were dissected, resuspended in triton lysis buffer and sonicated in a water bath for 15 min before being processing as described above. Lysates were heated at 70°C in NuPage LDS buffer (Thermo Fisher, NP0007) with 50 mM DTT. Samples were separated on 7.5% polyacrylamide gels, transferred to nitrocellulose and blocked with 5% skim-milk powder or 5% BSA in Tris-buffered saline with 0.05% Tween-20 (TBST) for 1 h at room temperature. Primary antibodies were diluted in blocking buffer and incubated overnight at 4°C. After 3 washes in TBST, membranes were incubated with peroxidase-linked secondary antibodies for 1 h at RT. Following an additional 3 washes, membranes were treated with Supersignal West Pico solution (Thermo Scientific, 34579). Images were acquired on an LAS-3000 system (Fuji Film).

Lambda-phosphatase treatment

Cells were lysed in modified RIPA lysis buffer 50 mM HEPES pH 8.0, 300 mM NaCl, 1% Triton X-100, 0.2% sodium deoxycholate, 0.05% SDS, 5 mM MgCl₂ supplemented with EDTA-free protease inhibitor tablet (Pierce, A32965) for 30 min on ice, spun down full speed at 4°C for 5 min and supernatants collected. Lysates were incubated with lambda phosphatase (NEB, P0753S) for 30 or 60 min (indicated in figure legends) at 30°C according to the manufacturer's instructions.

Ubiquitination assays

HA-tagged ubiquitin plasmid was co-transfected with Flag-tagged *Sox4/Sox11* or PCS2⁺ empty vector into 293T cells in 6 cm dishes for 48 h. Cells were treated for 4 h with 20 µM MG132 (Sigma-Aldrich, C2211) before being harvested in triton lysis buffer. A total of 200 µg protein was incubated with 20 µl FLAG beads (Sigma-Aldrich, A2220) overnight at 4°C with rotation. Beads were washed

4x with triton lysis buffer, resuspended in 20 mM Tris-HCl pH 7.5 buffer containing 0.1% SDS and heated for 5 min at 95°C to dissociate Sox binding partners. Cells were spun down, resuspended in triton lysis buffer and incubated a second time with 20 µl FLAG beads overnight at 4°C with rotation. Following 4 additional washes, NuPage LDS buffer supplemented with 50mM DTT was added to beads and samples were boiled at 70°C for 10 min.

In vitro kinase assays

Ten micrograms of *Sox4/Sox11* wild-type and mutant plasmids were transfected into 293T cells in 10-cm dishes for 48 h. Cells were lysed in 2 ml modified RIPA lysis buffer and incubated with 20 µl FLAG beads overnight at 4°C with rotation. Cells were then washed once with modified RIPA buffer, followed by two washes with high salt wash buffer (30 mM HEPES pH 8.0, 500 mM NaCl, 5 mM MgCl₂ supplemented with EDTA-free protease inhibitor tablet) and one wash with low salt wash buffer (30 mM HEPES pH 8.0, 500 mM NaCl, 5 mM MgCl₂ supplemented with EDTA-free protease inhibitor tablet). Cells were then resuspended in low salt wash buffer and treated with lambda phosphatase as described above.

For kinase assay, beads were washed once in wash buffer (30 mM HEPES-KOH pH 7.7, 10 mM MgCl₂, 0.2 mM β-mercaptoethanol) and equally divided in two 1.5-ml tubes. 10 nM GSK3β (Millipore, 14-306) or reaction buffer was added to the corresponding tube, and the reaction was started by adding 50 µM ATP containing 1 µCi of radiolabeled ³²P-γATP (Permin-Elmer, NEG502A001MC). Phosphorylation assays were performed at 37°C for 15 min in 30 µl of kinase buffer (30 mM HEPES-KOH pH 7.7, 10 mM MgCl₂, 1mM DTT, 0.2% BRUJ-35). Reactions were stopped by directly adding 10 µl of 4xSDS laemmli buffer, and samples were heated at 99°C for 7 min. 15 µl was loaded into a 10% SDS-PAGE and a 7.5% Phos-Tag gel (Alpha laboratories, 304-93526) followed by staining with Quick Coomassie® (Protein Ark, GEN-QC-STAIN-1L) and imaging of the dried gel with phosphorimager (Sapphire™ Biomolecular Imager, Azure Biosystems).

Antibodies

Rabbit polyclonal antibodies against *Ccny* and *Ccny11* were raised against synthetic peptides and affinity-purified as previously described (Davidson *et al*, 2009; Koch *et al*, 2015). No cross-reactivity with *Ccny11* was detected for the anti-*Ccny* antibody and vice versa. The rabbit polyclonal pLRP6 T1479 antibody is described in Davidson *et al* (2005). The *Sox4* and *Sox11* polyclonal guinea pig antibodies are described in Hoser *et al*, 2008. The *Sox4*-phospho polyclonal rabbit antibody is described below. All other antibodies used in this study are commercial and are described in the Appendix Table S2.

Sox4 phospho-antibody preparation

Rabbits were injected bi-weekly with AASpPAAGRC peptide conjugated to Imject Maleimide-Activated Blue Carrier Protein (Thermo Fisher, 77664), and serum was collected after 4 months. Rabbit antibody was purified by first passing through phosphopeptide immobilized to Sulfolink beads (Thermo Fisher, 20401) and then subtracted using non-phosphorylated peptide. Serum from 3 rabbits was

collected and purified, and the serum with the highest antibody yield was used for subsequent experiments. Rabbit housing, injections and serum collection was performed by Pineda Antikörper-Service (Berlin, Germany).

Immunofluorescence

Paraffin

Tissues were fixed overnight in 4% paraformaldehyde at 4°C, progressively dehydrated and embedded in paraffin. 7-µm thick sections were rehydrated, boiled in a pressure cooker for 2 min with citrate/EDTA buffer (10 mM sodium citrate, 5 mM Tris-HCl, 2 mM EDTA, pH 8.0) and blocked in blocking buffer (PBS solution containing 10% normal donkey serum, 1% BSA and 0.1% Triton X-100) for 30 min at room temperature. All primary antibodies were diluted in blocking buffer and applied overnight at 4°C. Secondary antibodies were diluted 1:500 in blocking buffer containing Hoechst 33258 dye (1:1,000)(Sigma-Aldrich, 861405) to stain DNA and applied at room temperature for 1 h. For histological analysis, 7-µm thick sections were stained with haematoxylin and eosin according to standard procedures.

Frozen sections

Tissues were fixed for 2 h in 4% paraformaldehyde at 4°C, incubated in 30% sucrose overnight, embedded in Tissue-Tek (OCT, Sakura, 4583) and frozen at -20°C. Sections of 8 µm thickness were washed briefly in PBS and then heated in a microwave for 5 min in sodium citrate buffer (10mM sodium citrate, 0.05% Tween pH 6.0). Blocking and antibody applications were performed as described above.

Cell culture

Cells were cultured on coverslips coated with poly D-lysine and fixed with 4% PFA at room temperature for 10 min. Following fixation cells were washed twice in PBS and then blocked and stained with indicated antibodies as described above.

TUNEL staining

TUNEL staining was performed with the Click-IT Plus TUNEL assay (Thermo Fisher, C10617) according to the manufacturer's instructions.

RNAScope in situ hybridization

Paraffin-embedded forebrain sections were processed for RNA *in situ* using the RNAScope 2.5 HD assay-RED kit (Advanced cell diagnostics, 322360) (Chromogenic and Fluorogenic) according to the manufacturer's instructions. The RNAScope probe used was *Axin2* (NM 015732, region 330-1287).

Quantification and statistical analysis

Sample sizes (individual embryos, litter numbers and wells (*in vitro* experiments)) are reported in each figure legend. All cell counts were performed in standardized microscopic fields (additional information in Appendix Methods) using either the Fiji cell counter plug in (quantifications done blindly) or user-defined macros (no

blinding for quantification). All statistical analyses were conducted using GraphPad Prism. Data normality was tested by Shapiro–Wilk normality test, and variances between groups were tested using F-test. Means between two groups were compared using two-tailed unpaired Student's *t*-test, and means between multiple groups were compared using one-way or two-way analysis of variance (ANOVA) followed by Tukey's multiple comparison tests. Statistical outliers were calculated using Grubb's test. Results are displayed as arithmetic mean \pm standard error of mean (SEM). Where indicated results are shown as fold change vs. controls. Statistically significant data are indicated as: **P* < 0.05, ***P* < 0.01, and ****P* < 0.001. Non-significant data are indicated as ns.

Note on terminology

The term "self-renewal" has been commonly used not only for asymmetric NPC divisions that result in the maintenance of the pool size of a given neural progenitor type (e.g. 1 AP \rightarrow 1 AP + 1 BP), but also for symmetric divisions of NPCs that increase the pool size of a given NPC type (e.g. 1 AP \rightarrow 2 APs, 1 BP \rightarrow 2 BPs). To clarify matters, we refer to the latter type of cell division as "increased self-renewal".

Data availability

This study includes no data deposited in external repositories.

Expanded View for this article is available online.

Acknowledgements

Expert technical help from the DKFZ core facilities for light microscopy, transgenics and the Central Animal Laboratory, and from the Biomedical Services Facility of the MPI-CBG, is gratefully acknowledged. We thank Elizabeth Sock for providing the Sox4 and Sox11 antibodies and Andrei Glinka for help with antibody purification. We also thank Hyeyoon Lee for designing the graphical abstract. This work was supported by the Deutsche Forschungsgemeinschaft (DFG), SFB 873. FDS was supported by the EMBO long-term fellowship ALTF 982-2018.

Author contributions

FDS and KZ conceived, performed and analysed experiments. JH supervised animal husbandry and assisted with experiments. EF performed the kinase assays. AP performed IUE experiments and cortical layer thickness measurements. MWB performed astral microtubule quantification. VV performed the RNAScope experiments, and AS helped with manuscript revision. WBH contributed by planning experiments and revising the manuscript. CN supervised all aspects of the project. FDS wrote the manuscript with input from all authors.

Conflict of interest

The authors declare that they have no conflict of interest.

References

Acebron SP, Karaulanov E, Berger BS, Huang YL, Niehrs C (2014) Mitotic Wnt signaling promotes protein stabilization and regulates cell size. *Mol Cell* 54: 663–674

- Acebron SP, Niehrs C (2016) β -catenin-independent roles of Wnt / LRP6 signaling. *Trends Cell Biol* 26: 956–967
- An W, Zhang Z, Zeng L, Yang Y, Zhu X, Wu J (2015) Cyclin Y is involved in the regulation of adipogenesis and lipid production. *PLoS One* 10: e0132721
- Arai Y, Pulvers JN, Haffner C, Schilling B, Nüsslein I, Calegari F, Huttner WB (2011) Neural stem and progenitor cells shorten S-phase on commitment to neuron production. *Nat Commun* 2: 154
- Asami M, Pilz GA, Ninkovic J, Godinho L, Schroeder T, Huttner WB, Götz M (2011) The role of Pax6 in regulating the orientation and mode of cell division of progenitors in the mouse cerebral cortex. *Development* 138: 5067–5078
- Balta EA, Schäffner I, Wittmann MT, Sock E, von Zweyendorf F, von Wittgenstein J, Steib K, HeimB KE, Häberle BM et al (2018b) Phosphorylation of the neurogenic transcription factor SOX11 on serine 133 modulates neuronal morphogenesis. *Sci Rep* 8: 16196
- Balta EA, Wittmann MT, Jung M, Sock E, Häberle BM, Heim B, von Zweyendorf F, Heptt J, von Wittgenstein J, Gloeckner CJ et al (2018a) Phosphorylation modulates the subcellular localization of SOX11. *Front Mol Neurosci* 8: 16196
- Bergslund M, Werme M, Malewicz M, Perlmann T, Muhr J (2006) The establishment of neuronal properties is controlled by Sox4 and Sox11. *Genes Dev* 20: 3475–3486
- Beurel E, Grieco SF, Jope RS (2015) Glycogen synthase kinase-3 (GSK3): regulation, actions, and diseases. *Pharmacol Ther* 148: 114–131
- Bhattaram P, Penzo-Méndez A, Kato K, Bandyopadhyay K, Gadi A, Taketo MM, Lefebvre V (2014) SOXC proteins amplify canonical WNT signaling to secure nonchondrocytic fates in skeletogenesis. *J Cell Biol* 207: 657–671
- Blom N, Gammeltoft S, Brunak S (1999) Sequence and structure-based prediction of eukaryotic protein phosphorylation sites. *J Mol Biol* 294: 1351–1362
- Borrell V, Calegari F (2014) Mechanisms of brain evolution: regulation of neural progenitor cell diversity and cell cycle length. *Neurosci Res* 86: 14–24
- Calegari F, Huttner WB (2003) An inhibition of cyclin-dependent kinases that lengthens, but does not arrest, neuroepithelial cell cycle induces premature neurogenesis. *J Cell Sci* 116: 4947–4955
- Caviness VS, Takahashi T, Nowakowski RS (1995) Numbers, time and neocortical neuronogenesis: a general developmental and evolutionary model. *Trends Neurosci* 18: 379–383
- Chen C, Lee GA, Pourmorady A, Sock E, Donoghue MJ (2015) Orchestration of neuronal differentiation and progenitor pool expansion in the developing cortex by SoxC genes. *J Neurosci* 35: 10629–10642
- Chen JF, Zhang Y, Wilde J, Hansen KC, Lai F, Niswander L (2014) Microcephaly disease gene Wdr62 regulates mitotic progression of embryonic neural stem cells and brain size. *Nat Commun* 5: 3885
- Chenn A, Walsh CA (2002) Regulation of cerebral cortical size by control of cell cycle exit in neural precursors. *Science* 297: 365–369
- Chiang SY, Wu HC, Lin SY, Chen HY, Wang CF, Yeh NH, Shih JH, Huang YS, Kuo HC, Chou SJ et al (2021) Usp11 controls cortical neurogenesis and neuronal migration through Sox11 stabilization. *Sci Adv* 7: eabc6093
- Davidson G, Shen J, Huang YL, Su Y, Karaulanov E, Bartscherer K, Hassler C, Stannek P, Boutros M, Niehrs C (2009) Cell cycle control of Wnt receptor activation. *Dev Cell* 17: 788–799
- Davidson G, Wu W, Shen J, Bilic J, Fenger U, Stannek P, Glinka A, Niehrs C (2005) Casein kinase 1 γ couples Wnt receptor activation to cytoplasmic signal transduction. *Nature* 438: 867–872
- Dehay C, Kennedy H (2007) Cell-cycle control and cortical development. *Nat Rev Neurosci* 8: 438–450

- Delaunay D, Cortay V, Patti D, Knoblauch K, Dehay C (2014) Mitotic spindle asymmetry: a Wnt/PCP-regulated mechanism generating asymmetrical division in cortical precursors. *Cell Rep* 6: 400–414
- Delaunay D, Kawaguchi A, Dehay C, Matsuzaki F (2017) Division modes and physical asymmetry in cerebral cortex progenitors. *Curr Opin Neurobiol* 42: 75–83
- Ding W, Wu Q, Sun L, Pan NC, Wang X (2019) Cenj regulates cilia disassembly and neurogenesis in the developing mouse cortex. *J Neurosci* 39: 1994–2010
- Draganova K, Zemke M, Zurkirchen L, Valenta T, Cantù C, Okoniewski M, Schmid MT, Hoffmans R, Götz M, Basler K *et al* (2015) Wnt/ β -catenin signaling regulates sequential fate decisions of murine cortical precursor cells. *Stem Cells* 33: 170–182
- Florio M, Huttner WB (2014) Neural progenitors, neurogenesis and the evolution of the neocortex. *Development* 141: 2182–2194
- García de Herreros A, Duñach M (2019) Intracellular signals activated by canonical Wnt ligands independent of GSK3 inhibition and β -catenin stabilization. *Cells* 8: 1148
- Goel S, Chin EN, Fakhraldeen SA, Berry SM, Beebe DJ, Alexander CM (2012) Both LRP5 and LRP6 receptors are required to respond to physiological Wnt ligands in mammary epithelial cells and fibroblasts. *J Biol Chem* 287: 16454–16466
- Götz M, Huttner WB (2005) The cell biology of neurogenesis. *Nat Rev Mol Cell Biol* 6: 777–788
- Gulacsi AA, Anderson SA (2008) β -catenin-mediated Wnt signaling regulates neurogenesis in the ventral telencephalon. *Nat Neurosci* 11: 1383–1391
- Habib SJ, Chen BC, Tsai FC, Anastassiadi K, Meyer T, Betzig E, Nusse R (2013) A localized Wnt signal orients asymmetric stem cell division *in vitro*. *Science* 339: 1445–1448
- Harrison-Uy SJ, Pleasure SJ (2012) Wnt signaling and forebrain development. *Cold Spring Harb Perspect Biol* 4: a008094
- Hinze L, Pfirrmann M, Karim S, Degar J, McGuckin C, Vinjamur D, Sacher J, Stevenson KE, Neuberger DS, Orellana E *et al* (2019) Synthetic lethality of Wnt pathway activation and asparaginase in drug-resistant acute leukemias. *Cancer Cell* 35: 664–676
- Hirabayashi Y, Itoh Y, Tabata H, Nakajima K, Akiyama T, Masuyama N, Gotoh Y (2004) The Wnt/ β -catenin pathway directs neuronal differentiation of cortical neural precursor cells. *Development* 131: 2791–2801
- Hornbeck PV, Kornhauser JM, Tkachev S, Zhang B, Skrzypek E, Murray B, Latham V, Sullivan M (2012) PhosphoSitePlus: a comprehensive resource for investigating the structure and function of experimentally determined post-translational modifications in man and mouse. *Nucleic Acids Res* 40: 261–270
- Hoser M, Potzner MR, Koch JMC, Bösl MR, Wegner M, Sock E (2008) Sox12 deletion in the mouse reveals non reciprocal redundancy with the related Sox4 and Sox11 transcription factors. *Mol Cell Biol* 28: 4675–4687
- Hoshiba Y, Toda T, Ebisu H, Wakimoto M, Yanagi S, Kawasaki H (2016) Sox11 balances dendritic morphogenesis with neuronal migration in the developing cerebral cortex. *J Neurosci* 36: 5775–5784
- Hu WF, Chahrouh MH, Walsh CA (2014) The diverse genetic landscape of neurodevelopmental disorders. *Annu Rev Genomics Hum Genet* 15: 195–213
- Huang YL, Anvarian Z, Döderlein G, Acebron SP, Niehrs C (2015) Maternal Wnt/STOP signaling promotes cell division during early *Xenopus* embryogenesis. *Proc Natl Acad Sci USA* 112: 5732–5737
- Huttner WB, Kosodo Y (2005) Symmetric versus asymmetric cell division during neurogenesis in the developing vertebrate central nervous system. *Curr Opin Cell Biol* 17: 648–657
- Israsena N, Hu M, Fu W, Kan L, Kessler JA (2004) The presence of FGF2 signaling determines whether β -catenin exerts effects on proliferation or neuronal differentiation of neural stem cells. *Dev Biol* 268: 220–231
- Kelly OG, Pinson KI, Skarnes WC (2004) The Wnt co-receptors Lrp5 and Lrp6 are essential for gastrulation in mice. *Development* 131: 2803–2815
- Kim WY, Wang X, Wu Y, Doble BW, Patel S, Woodgett JR, Snider WD (2009) GSK-3 is a master regulator of neural progenitor homeostasis. *Nat Neurosci* 12: 1390–1397
- Koch S, Acebron SP, Herbst J, Hatiboglu G, Niehrs C (2015) Post-transcriptional Wnt signaling governs epididymal sperm maturation. *Cell* 163: 1225–1236
- Konno D, Shioi G, Shitamukai A, Mori A, Kiyonari H, Miyata T, Matsuzaki F (2008) Neuroepithelial progenitors undergo LGN-dependent planar divisions to maintain self-renewability during mammalian neurogenesis. *Nat Cell Biol* 10: 93–101
- Kosodo Y, Röper K, Haubensak W, Marzesco AM, Corbeil D, Huttner WB (2004) Asymmetric distribution of the apical plasma membrane during neurogenic divisions of mammalian neuroepithelial cells. *EMBO J* 23: 2314–2324
- Kriegstein AR, Götz M (2003) Radial glia diversity: a matter of cell fate. *Glia* 43: 37–43
- Kuwahara A, Hirabayashi Y, Knoepfler PS, Taketo MM, Sakai J, Kodama T, Gotoh Y (2010) Wnt signaling and its downstream target N-myc regulate basal progenitors in the developing neocortex. *Development* 137: 1035–1044
- LaMonica BE, Lui JH, Hansen DV, Kriegstein AR (2013) Mitotic spindle orientation predicts outer radial glial cell generation in human neocortex. *Nat Commun* 4: 1665
- Lange C, Huttner WB, Calegari F (2009) Cdk4/CyclinD1 overexpression in neural stem cells shortens G1, delays neurogenesis, and promotes the generation and expansion of basal progenitors. *Cell Stem Cell* 5: 320–331
- Lian G, Dettenhofer M, Lu J, Downing M, Chenn A, Wong T, Sheen V (2016) Filamin A- and formin 2-dependent endocytosis regulates proliferation via the canonical wnt pathway. *Development* 143: 4509–4520
- Lian G, Wong T, Lu J, Hu J, Zhang J, Sheen V (2019) Cytoskeletal associated filamin a and RhoA affect neural progenitor specification during mitosis. *Cereb Cortex* 29: 1280–1290
- Lin Y-C, Haas A, Bufe A, Parbin S, Hennecke M, Voloshanenko O, Gross J, Boutros M, Acebron SP, Bastians H (2020) Wnt10b-GSK3 β -dependent Wnt/STOP signaling prevents aneuploidy in human somatic cells. *Life Sci Alliance* 4: e202000855
- Liu J, Cui Z, Wang F, Yao Y, Yu G, Liu J, Cao D, Niu S, You M, Sun Z *et al* (2019) Lrp5 and Lrp6 are required for maintaining self-renewal and differentiation of hematopoietic stem cells. *FASEB J* 33: 5615–5625
- Lizarraga SB, Margossian SP, Harris MH, Campagna DR, Han AP, Blevins S, Mudbhary R, Barker JE, Walsh CA, Fleming MD (2010) Cdk5rap2 regulates centrosome function and chromosome segregation in neuronal progenitors. *Development* 137: 1907–1917
- Lois C, Hong EJ, Pease S, Brown EJ, Baltimore D (2002) Germline transmission and tissue-specific expression of transgenes delivered by lentiviral vectors. *Science* 295: 868–872
- Lu MS, Johnston CA (2013) Molecular pathways regulating mitotic spindle orientation in animal cells. *Development* 140: 1843–1856
- Lui JH, Hansen DV, Kriegstein AR (2011) Development and evolution of the human neocortex. *Cell* 146: 18–36
- Machon O, Backman M, Machonova O, Kozmik Z, Vacik T, Andersen L, Krauss S (2007) A dynamic gradient of Wnt signaling controls initiation of neurogenesis in the mammalian cortex and cellular specification in the hippocampus. *Dev Biol* 311: 223–237

- Machon O, Van Den Bout CJ, Backman M, Kemler R, Krauss S (2003) Role of β -catenin in the developing cortical and hippocampal neuroepithelium. *Neuroscience* 122: 129–143
- Madan B, Harmston N, Nallan G, Montoya A, Faull P, Petretto E, Virshup DM (2018) Temporal dynamics of Wnt-dependent transcriptome reveal an oncogenic Wnt/MYC/ribosome axis. *J Clin Invest* 128: 5620–5633
- Malatesta P, Hartfuss E, Götz M (2000) Isolation of radial glial cells by fluorescent-activated cell sorting reveals a neural lineage. *Development* 127: 5253–5263
- Melnik S, Dvornikov D, Müller-Decker K, Depner S, Stannek P, Meister M, Warth A, Thomas M, Muley T, Risch A et al (2018) Cancer cell specific inhibition of Wnt/ β -catenin signaling by forced intracellular acidification. *Cell Discov* 4: 37
- Molnár Z, Clowry GJ, Šestan N, Alzu'bi A, Bakken T, Hevner RF, Hüppi PS, Kostović I, Rakic P, Anton Es et al (2019) New insights into the development of the human cerebral cortex. *J Anat* 235: 432–451
- Mora-Bermúdez F, Huttner WB (2015) Novel insights into mammalian embryonic neural stem cell division: focus on microtubules. *Mol Biol Cell* 26: 4302–4306
- Mora-Bermúdez F, Matsuzaki F, Huttner WB (2014) Specific polar subpopulations of astral microtubules control spindle orientation and symmetric neural stem cell division. *Elife* 3: e02875
- Munji RN, Choe Y, Li G, Siegenthaler JA, Pleasure SJ (2011) Wnt signaling regulates neuronal differentiation of cortical intermediate progenitors. *J Neurosci* 31: 1676–1687
- Mutch CA, Schulte JD, Olson E, Chenn A (2010) Beta-catenin signaling negatively regulates intermediate progenitor population numbers in the developing cortex. *PLoS One* 5: e12376
- Noctor SC, Flint AC, Weissman TA, Dammerman RS, Kriegstein AR (2001) Neurons derived from radial glial cells establish radial units in neocortex. *Nature* 409: 714–720
- Nusse R, Clevers H (2017) Wnt/ β -catenin signaling, disease, and emerging therapeutic modalities. *Cell* 169: 985–999
- Palozola KC, Lerner J, Zaret KS (2019) A changing paradigm of transcriptional memory propagation through mitosis. *Nat Rev Mol Cell Biol* 20: 55–64
- Pemberton K, Mersman B, Xu F (2018) Using ImageJ to assess neurite outgrowth in mammalian cell cultures: research data quantification exercises in undergraduate neuroscience lab. *J Undergrad Neurosci Educ* 16: A186–A194
- Pilaz LJ, McMahon JJ, Miller EE, Lennox AL, Suzuki A, Salmon E, Silver DL (2016) Prolonged mitosis of neural progenitors alters cell fate in the developing brain. *Neuron* 89: 83–99
- Qu Q, Sun G, Murai K, Ye P, Li W, Asulime G, Cheung Y-T, Shi Y (2013) Wnt7a regulates multiple steps of neurogenesis. *Mol Cell Biol* 33: 2551–2559
- Rakic P (1995) A small step for the cell, a giant leap for mankind: a hypothesis of neocortical expansion during evolution. *Trends Neurosci* 18: 383–388
- Rakic P (2009) Evolution of the neocortex: a perspective from developmental biology. *Nat Rev Neurosci* 10: 724–735
- Rosenbloom AB, Tarczynski M, Lam N, Kane RS, Bugaj LJ, Schaffer DV (2020) β -Catenin signaling dynamics regulate cell fate in differentiating neural stem cells. *Proc Natl Acad Sci USA* 117: 28828–28837
- Stolz A, Neufeld K, Ertych N, Bastians H (2015) Wnt-mediated protein stabilization ensures proper mitotic microtubule assembly and chromosome segregation. *EMBO Rep* 16: 490–499
- Sugioka K, Mizumoto K, Sawa H (2011) Wnt regulates spindle asymmetry to generate asymmetric nuclear β -catenin in *C. elegans*. *Cell* 146: 942–954
- Sun D, Zhou X, Yu HL, He XX, Guo WX, Xiong WC, Zhu XJ (2017) Regulation of neural stem cell proliferation and differentiation by kinesin family member 2a. *PLoS One* 12: e0179047
- Sun T, Hevner RF (2014) Growth and folding of the mammalian cerebral cortex: from molecules to malformations. *Nat Rev Neurosci* 15: 217–232
- Taelman VF, Dobrowolski R, Plouhinec JL, Fuentealba LC, Vorwald PP, Gumper I, Sabatini DD, De Robertis EM (2010) Wnt signaling requires sequestration of glycogen synthase kinase 3 inside multivesicular endosomes. *Cell* 143: 1136–1148
- Taverna E, Götz M, Huttner WB (2014) The cell biology of neurogenesis: toward an understanding of the development and evolution of the neocortex. *Annu Rev Cell Dev Biol* 30: 465–502
- Turrero García M, Chang Y, Arai Y, Huttner WB (2016) S-phase duration is the main target of cell cycle regulation in neural progenitors of developing ferret neocortex. *J Comp Neurol* 524: 456–470
- Viti J, Gulacsi A, Lillien L (2003) Wnt regulation of progenitor maturation in the cortex depends on Shh or fibroblast growth factor 2. *J Neurosci* 23: 5919–5927
- Woodhead GJ, Mutch CA, Olson EC, Chenn A (2006) Cell-autonomous β -catenin signaling regulates cortical precursor proliferation. *J Neurosci* 26: 12620–12630
- Wrobel CN, Mutch CA, Swaminathan S, Taketo MM, Chenn A (2007) Persistent expression of stabilized β -catenin delays maturation of radial glial cells into intermediate progenitors. *Dev Biol* 309: 285–297
- Xie Y, Jüschke C, Esk C, Hirotsune S, Knoblich JA (2013) The phosphatase PP4c controls spindle orientation to maintain proliferative symmetric divisions in the developing neocortex. *Neuron* 79: 254–265
- Yingling J, Youn YH, Darling D, Toyo-oka K, Pramparo T, Hirotsune S, Wynshaw-Boris A (2008) Neuroepithelial stem cell proliferation requires LIS1 for precise spindle orientation and symmetric division. *Cell* 132: 474–486
- Zechner D, Fujita Y, Hülsken J, Müller T, Walther I, Taketo MM, Crenshaw EB, Birchmeier W, Birchmeier C (2003) β -catenin signals regulate cell growth and the balance between progenitor cell expansion and differentiation in the nervous system. *Dev Biol* 258: 406–418
- Zeng L, Cai C, Li S, Wang W, Li Y, Chen J, Zhu X, Zeng YA (2016) Essential roles of cyclin Y-like 1 and cyclin Y in dividing Wnt-responsive mammary stem/progenitor cells. *PLoS Genet* 12: e1006055
- Zhong Z, Baker JJ, Zylstra-Diegel CR, Williams BO (2012) Lrp5 and Lrp6 play compensatory roles in mouse intestinal development. *J Cell Biochem* 113: 31–38
- Zhou CJ, Borello U, Rubenstein JLR, Pleasure SJ (2006) Neuronal production and precursor proliferation defects in the neocortex of mice with loss of function in the canonical Wnt signaling pathway. *Neuroscience* 142: 1119–1131



License: This is an open access article under the terms of the Creative Commons Attribution-NonCommercial-NoDerivs License, which permits use and distribution in any medium, provided the original work is properly cited, the use is non-commercial and no modifications or adaptations are made.